Analysis of a Duo-Selecting Membrane Reactor for the Water-Gas Shift

by

AliciA Jillian Jackson Hardy

Submitted to the Department of Mechanical Engineering
in partial fulfillment of the requirements for the degree of

Master of Science in Mechanical Engineering

at the

MASSACHUSETTS INSTITUTE OF TECHNOLOGY

May 2004 [June 2004]

Author .....
Department of Mechanical Engineering
7 May 2004

Certified by.....
Ernest G. Cravalho
Professor of Mechanical Engineering
Thesis Supervisor

Accepted by.....
Ain A. Sonin
Graduate Officer

Analysis of a Duo-Selecting Membrane Reactor for the Water-Gas Shift

by

AliciA Jillian Jackson Hardy

Submitted to the Department of Mechanical Engineering
on 7 May 2004, in partial fulfillment of the
requirements for the degree of
Master of Science in Mechanical Engineering

Abstract

The water-gas shift reaction is an exothermic and reversible catalytic process that converts carbon monoxide and water (steam) to hydrogen and carbon dioxide. In regard to energy-related issues, the water-gas shift is part of the process of reforming hydrocarbons to produce hydrogen suitable for fuel cells; carbon monoxide poisons the low temperature fuel cells (phosphoric acid and polymer electrolyte membrane fuel cells) and must therefore be removed. The reaction is limited by thermodynamic equilibrium at higher temperatures, while kinetics are unfavorable at the lower temperatures. Current commercial technology uses at least two adiabatic beds with cooling between the beds to address this issue. The first bed is a high temperature shift in which reaction rates are high, and the second is a low temperature shift where final equilibrium conversions are high. The high temperature shift is made less unfavorable thermodynamically by reacting the gas with an excess of steam. Membrane reactors are expected to eliminate the thermodynamics/kinetics trade-off by separating either the hydrogen or the carbon dioxide while the forward reaction is in progress. In such a reactor, excess steam might not be required; commercial catalysts are not well studied under conditions in which the pressure is high and the feed is near stoichiometric, as they would be in membrane reactor. Further study of old and new catalysts under these conditions is necessary step toward making membrane reactors marketable. There is a whole body of literature regarding new catalysts for the water-gas shift, and there are certainly other methods to produce hydrogen besides steam reforming natural gas. However, in order to be marketable now, fuel cells need to use primary fuel sources from existing production and distribution networks (such as natural gas, gasoline, diesel fuel and jet fuel), and the exhaustive body of knowledge that has been gathered over the past century regarding today's common water-gas shift catalysts suggests that there are under-investigated design options to pursue. In this vain, the current work studies how to more efficiently use the most common and best understood high temperature water-gas shift catalyst: ferrochrome Fe_3O_4 with a Cr_2O_3 promoter. The current work suggests the application of this catalyst in a membrane reactor environment in which the partial pressures of both hydrogen and carbon dioxide are both low.

Thesis Supervisor: Ernest G. Cravalho
Title: Professor of Mechanical Engineering

Acknowledgments

I would like to acknowledge Professors Cravalho, Brisson, Smith, Sonin, Ghoniem, M^{c}Kinley and Mikić, all of whom have very positively influenced me during my development as a graduate student in the Master's program and while I assembled this body of work.

I would also like to acknowledge the graduate students with whom I have worked most closely and from whom I have consistently received support and encouragement: Franklin Miller, Fritz Pierre, Omar Roushdy, Matthew Traum, Sofy Tarud, Joan Tisdale, and Przemek Jamroz.

Contents

List of Figures

List of Tables

Chapter 1

Introduction

1.1 Hydrogen Production Today

1.1.1 Consumption Around the World

Increasingly more research opportunities to improve the process of hydrogen production arise as nations around the world continue preparation for the transition to a fuel infrastructure in which the production, transport and consumption of hydrogen are a focal point. In 1996, three trillion cubic feet of hydrogen were consumed in the United States, where hydrogen is used in a number of different commercial applications. Today's largest consumers are ammonia production facilities (40.3%), oil refineries (37.3%), and producers of methanol (10.0%) [1]. International consumption of hydrogen follows a similar trend, with ammonia production accounting for 62.4% of the world's hydrogen, and oil refining and methanol production consuming 24.3% and 8.7% respectively [1]. Because such large amounts of hydrogen are required in these stationary applications, the hydrogen is typically produced by the hydrogen-consuming plant, and the most common means of production is currently the steam reforming of natural gas. As a result of the fast-growing fuel cell industry, hydrogen usage is expected to eventually become prevalent on the level of the individual consumer, in laptops, vehicles, cell phones and various home appliances. Even for the portable applications, it is expected that the steam reforming of natural gas will be among the primary methods of producing hydrogen

and hydrogen-rich "transition" fuels[1]. The process is an old and well-established technology but continues undergoing development as the challenges of new applications are met.

1.1.2 Assessment of a Steam-Methane Reforming Plant

Spath and Mann conducted a life-cycle assessment of a steam methane reforming hydrogen plant whose block diagram is shown in Figure 1.1. Natural gas feedstock is hydrogenated before being desulfurized on a zinc-oxide bed so that the catalysts in subsequent reactors are not fouled. In the first reactor, the catalytic steam reformer, the natural gas is cracked by steam and decomposes into hydrogen and carbon monoxide. Two shift reactors follow the catalytic steam reformer to convert the carbon monoxide present in the stream to more hydrogen and carbon dioxide, which will ultimately be sequestered. As will be discussed in later chapters, two shift reactors are used in this traditional design so as to convert as much of the carbon monoxide as possible. The pressure swing adsorption system runs at near vacuum pressures and separates the hydrogen from the other gases in the stream.

The assessment by Spath and Mann highlighted several opportunities for improvement in this process of producing hydrogen, from the operations well upstream of the plant to the final purification steps leading to the industrial-grade hydrogen at the exit stream. Data describing the hydrogen plant in the assessment are shown in Table 1.1 (Spath and Mann 2001).

It should be noted that the plant efficiency in this assessment is defined as follows [1]:

$$\eta_{\text{plant}} = \frac{\text{energy in product hydrogen } + \text{ 4.8 MPa steam energy (required)}}{\text{natural gas energy } + \text{ electricity } + \text{ 2.6 MPa steam energy (required)}}$$

This definition assumes that all required steam for the operation of the plant is produced internally, and that all generated steam is used by another operation. If the 4.8 MPa steam were considered a waste product, the plant efficiency would drop from 89.1% to to 69.1%.

[1]The hope for the distant future is to generate energy using renewable resources, such as hydroelectric, solar and wind. Any non-renewable fuel, such as natural gas, might therefore be termed "transitional." To this end, hydrogen might also be considered a transitional fuel if it is produced via the reforming of a (non-renewable) hydrocarbon

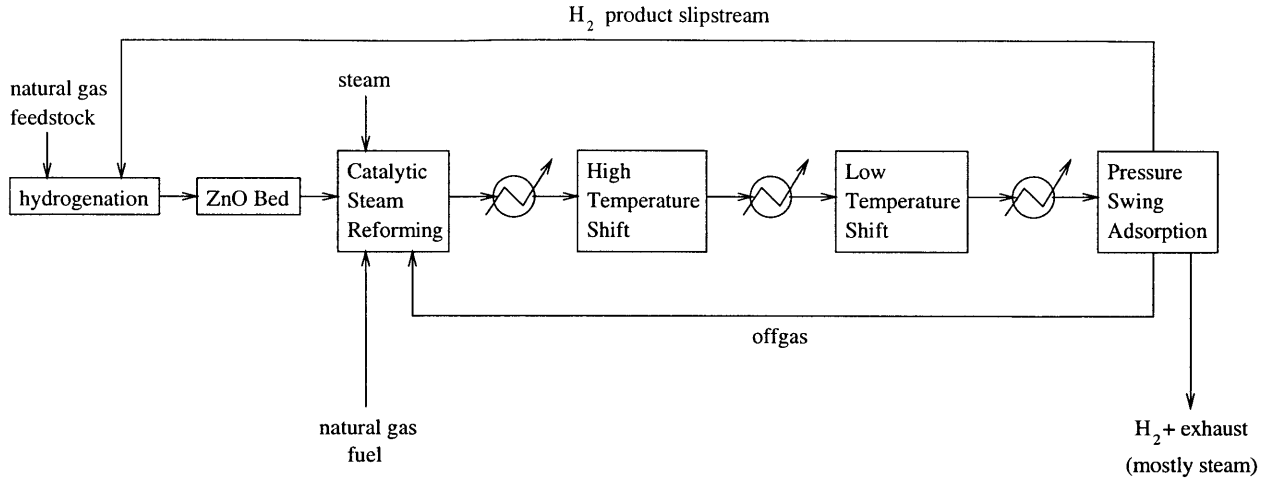

Figure 1.1: Block diagram of the hydrogen plant (Spath and Mann, 2002).

Design Parameter	**Data**
Plant Size (hydrogen production capacity)	1.5 million Nm^3/day
Hydrogen purity	Industrial grade (>99.95 mol% H_2)
Average operating capacity factor	90%
Natural gas consumed at 100% operating capacity	392 Mg/day (feed)
Steam requirement (2.6 MPa or 280 psi) at 100% operating capacity	1293 Mg/day
Steam production (4.8 MPa or 700 psi) at 100% operating capacity	1858 Mg/day
Electricity requirement at 100% operating capacity	153311 MJ/day
Hydrogen plant energy efficiency (higher heating value basis)	89%

Table 1.1: Steam Methane Reforming Plant Data

Economy of Steam

Management of steam is a huge area of interest for researchers aiming to improve the performance of the plant. Spath and Mann reported the following notable characteristics regarding steam consumption.

Per kilogram of hydrogen produced, 19.8 liters of water are consumed. 95% of this total is consumed during operation of the hydrogen plant: 24% of the total is consumed during the steam cracking of methane and water-gas shift reactions (to be discussed in detail in subsequent chapters), and over 71% of the total is consumed during the production of the 4.8 MPa steam. The economy of steam within a hydrogen plant must be managed very carefully and the internal components which require excess steam are undergoing continual design improvements. As will be discussed at length, the current work suggests that the high temperature shift reactor, low temperature shift reactor and pressure swing adsorption system can be replaced by a single membrane reactor that can operate at high pressure and require significantly less excess steam.

Greenhouse Gas Emissions

Other opportunities to improve hydrogen production via steam methane reforming abound. Managing the emission of greenhouse gases is another area of research receiving focused attention. One of the great selling points for fuel cells today is that they are environmentally friendly because they run on hydrogen, a clean, carbon-free fuel. While this is true, the production of hydrogen via steam methane reforming can be as environmentally unfriendly as the combustion of a hydrocarbon. Table 1.2 is a summary of the average air emissions involved in this process, from the extraction of natural gas from the earth to the production of purified hydrogen [1]. Carbon dioxide is the most important greenhouse gas and is emitted from the system in greatest abundance, but methane and nitrous oxide also contribute to global warming. In fact, the potential of CH_4 and N_2O to contribute to the warming of the atmosphere is 21 and 310 times higher than CO_2 respectively over a period of 100 years according to the Intergovernmental Panel on Climate Change (IPCC) [2]. Thus, Spath and Mann normalized the global warming potential of the greenhouse gases emitted by the system and associated processes to a CO_2-equivalence (Table 1.3).

Per kilogram of hydrogen produced, the breakdown of greenhouse gas emissions is as follows:

Air Emission	System Total (g/kg H_2)	% of total	% from C and D	% from P and T	% from EG	% from PO	% from AO
Benzene (C_6H_6)	1.4	0.0	0.0	110.9	0.0	0.0	-10.9
Carbon Dioxide (CO_2)	10620.6	99.0	0.4	14.8	2.5	83.7	-1.5
Carbon Monoxide (CO)	5.7	0.1	2.0	106.3	0.7	1.4	-10.4
Methane (CH_4)	59.8	0.6	0.0	110.8	0.0	0.0	-10.9
Nitrogen oxides (NO_x as NO_2)	12.3	0.1	1.8	90.3	9.5	7.3	-8.9
Nitrous oxide (N_2O)	0.04	0.0	7.3	37.6	58.7	0.0	-3.7
Non-methane hydrocarbons	16.8	0.2	1.7	89.8	14.5	0.0	-6.0
Particulates	2.0	0.0	64.5	25.2	11.6	1.1	-2.5
Sulfur oxides (SO_x as SO_2)	9.5	0.1	13.5	68.3	24.9	0.0	-6.7

Table 1.2: Average Air Emissions [1]. C and D = construction and decommissioning; P and T = production and transport; EG = electricity generation; PO = plant operation; AO = avoided operations

Greenhouse gas	Amount emitted (g/kg H_2)	Global warming potential relative to CO_2	g CO_2-equivalent/kg H_2	Percent contribution to system global warming potential
CO_2	10621	1	10621	89.3
CH_4	60	21	1256	10.6
N_2O	0.04	310	11	0.1
			11888	

Table 1.3: Greenhouse Gases Emissions and Global Warming Potential [1]

2972g CO_2-equivalent is emitted during the process of natural gas production and distribution, 273g CO_2-equivalent is emitted during electricity generation, 41g CO_2-equivalent is emitted during construction and decommissioning[2], 293g CO_2-equivalent are subtracted from the total emissions as a result of the avoided operations[3], and 8895g CO_2-equivalent are emitted during operation of the hydrogen plant [1].

In their life-cycle assessment, Spath and Mann also note the consumption of natural resources involved, the most notable being the 3642 grams of natural gas consumed per kilogram of H_2 produced. They also note the production of solid waste, which averages approximately 201 grams per kilogram of H_2. Continued research and development efforts in the area of hydrogen production via steam-methane reforming and fuel cells aim to lower these numbers.

1.2 Some Research Efforts in Hydrogen Production and Reformer Technology

The list of research in the areas of fuel cells, hydrogen production and reformer technology is virtually limitless. The works mentioned here are a few of the very many.

1.2.1 Additional Hydrogen Sources

One research effort in the area of hydrogen production aims to broaden our search for hydrogen sources. Significantly more hydrogen will have to be produced in order for hydrogen to become a significant part of the present day fuel infrastructure in the United States and around the world. According to the U.S. DOE 1994 fuel use numbers, the rate of household and transportation fuel use is at a hydrogen equivalent of 0.25 billion kg/day, which is 5.5 times the current rate of hydrogen production in this country. In order to meet the nation's fuel usage demands, hydrogen will have to be recovered from all possible gas streams, including those with low partial pressures of hydrogen. In a recent submission to the DOE, Heung describes how to recover hydrogen from such gas streams by using composite materials comprised of metal hydride particles encapsulated in a porous silica

[2]Construction and decommissioning includes plant construction and decommissioning as well as the construction of the natural gas pipeline.

[3]Avoided operations produce and consume steam as needed.

matrix [3].

1.2.2 On-board Hydrogen Production

There is a body of literature available regarding the on-board production of hydrogen that meets the transient response demands of gasoline-fueled fuel cell vehicles. On-board hydrogen production systems typically consist of a reformer, a high-temperature shift, a low-temperature shift and preferential oxidation. Such systems are bulky and expensive, two main reasons why they are not yet marketable. Brooks, et al. have addressed the problem of size with a clever microchannel fuel processor design that is capable of reaching full power from start-up in fifteen minutes at 20°C [14]. The goal of the work is to have the system reach full power in less than one minute, and the research team from Pacific Northwest National Laboratory expects to meet this goal by redesigning the reactors using low pressure drop concepts. Betta and Thompson are also developing fast-starting fuel processors that will produce hydrogen suitable for PEM fuel cells, which might become more popular in a vehicular application [15, 16].

Also in the area of hydrogen production is the work by Muradov [8]. The goal of his work is to improve production efficiency, reduce overall production cost, and also obviate the concurrent production of carbon oxides and other undesirables such as greenhouse emissions. The approach involves thermocatalytic decomposition of hydrocarbon feedstocks (such as methane) over carbon-based catalysts in an air/water-free environment. This work points us in the direction of making the production of hydrogen as environmentally friendly as fuel cell operation.

1.2.3 Membrane Development

The development of membrane reactors is a focal point in the effort to improve hydrogen production; membrane reactor development is, in turn, heavily tied to the development of suitable membranes and catalysts. To this end, the development of membranes that successfully select a molecule as large as carbon-dioxide is currently in accelerated stages. Sandia National Laboratories has successfully synthesized defect-free thin film zeolite membrane with different selectivities for various gas molecules [4]. The pore sizes and shapes are defined crytallographically with less than 1 Å deviation to allow for size exclusion of very similarly sized molecules including CO_2. Another such advancement in membrane technology is the work by Ho [5]. The objective of his work is to produce

a CO_2-selective membrane by incorporating amines in polyvinylalcohol networks. The amines will facilitate the transport of the carbon-dioxide, and the polymer network will reject the hydrogen. A CO_2-selective hydrotalcite (ceramic) membrane is being developed by a UCLA project team in conjunction with Media and Process Technology, Inc. These works will offer notable options in the design of membrane reactors and promise to help greatly with the final purification stages of hydrogen production. CO_2-selective membrane options are of particular import to the current work, which is based upon the ability to selectively remove both hydrogen and carbon-dioxide.

1.2.4 Cost as Motivation

The issue of cost is a large motivating factor in the accelerated development of membrane reactor technology and research. Over several studies, Directed Technologies, Inc. has analyzed the costs of representative hydrogen fueling appliances to supply the early-introduction hydrogen powered fuel cell vehicles and the cost of the hydrogen produced by these hydrogen fueling appliances [9]. The goal of the work was to determine the most practical and economically feasible plan for the supply of 10 Quads/year of renewable hydrogen for transportation applications in 2030-2050. Some of the key results of this work, summarized in Table 1.4, identified a steam methane reformer system with a pressure swing adsorption device as the most cost efficient means of producing hydrogen. Purchasing hydrogen produced by this method would be equivalent to paying \$1.55/gallon for gasoline, which is comparable to the current retail market price in the United States today. Alternatives considered in this work were autothermal reforming with a pressure swing adsorption device, steam methane reforming in a membrane reactor and autothermal reforming in a membrane reactor. The most costly means of producing hydrogen would be autothermal reforming with a membrane reactor. Buying hydrogen produced this way would be equivalent to paying \$1.96 per gallon of gasoline.

Hydrogen production systems that include pressure swing adsorption are a mature technology whose potential for design improvement is limited. Also very importantly, pressure swing adsorption systems are part of a hydrogen purification process that requires multiple large heat exchangers and pumps. The amount of hardware required to purify the hydrogen stream could be substantially lessened by the use of membrane reactors and no pressure swing adsorption. Membrane reactors for use in hydrogen production are relatively nascent and, after further development, are expected

to replace the traditional reactor designs. The benefits of membrane reactors will be discussed in detail in the next chapter.

Cost	**SMR/ PSA**	**ATR/ PSA**	**SMR/ Membrane**	**ATR/ Membrane**
Hydrogen (in $/kg)	$ 3.38	$ 3.59	$ 3.74	$ 4.28
Gasoline Equivalent (in $/gal)	$ 1.55	$ 1.65	$ 1.72	$ 1.96

Table 1.4: Cost of hydrogen produced from the 115 kg/day hydrogen fueling appliances options [9].

Chapter 2

Membrane Reactors

Membrane reactors are more efficient than traditional reactors because they combine in one unit a reactor that creates products and a permselective membrane, which is a membrane that selectively removes one or more of these products. The result is a more compact design capable of achieving significantly higher conversion of equilibrium-limited reactions. Extraction of one of the products drives the forward reaction toward completion because the equilibrium limit is not reached until the gas stream exits the reactor. See Figure 2.1, a schematic of a membrane reactor for hydrocarbon reforming that removes the product H_2 from the main gas stream. As will be discussed below, membrane reactors also allow for longer residence times of the reactants, thus decreasing the amount of catalyst required to achieve a given extent of reaction[1]. Buxbaum points out an even greater advantage of the membrane reactor: it allows a wider range of temperatures and pressures at which the forward reaction can proceed [11].

Membrane reactors are open systems in which the number of moles of gas in the reactor is not purely a function of the number of moles entering the reactor, as is the case in a traditional plug-flow reactor. Membrane reactors fundamentally change the pressure dependence of the conversion rate of the forward reaction. A reaction that is more efficient at low pressure in a traditional reactor preferentially takes place at high pressures in a membrane reactor. This final advantage greatly simplifies an otherwise enormously complex fluids/thermochemistry/kinetics problem, which typically requires a large reactor and substantial heat transfer area.

[1]This latter advantage was studied by Armor [10].

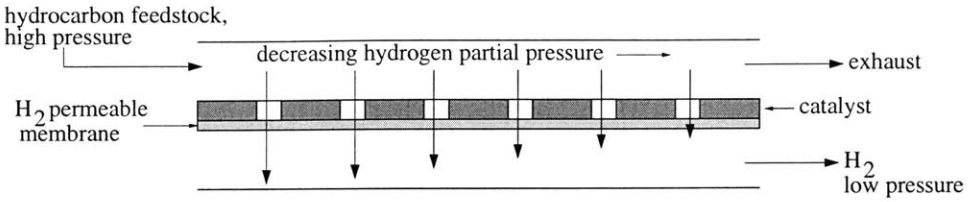

Figure 2.1: Schematic of a reforming membrane reactor. A porous catalyst is backed by a hydrogen-permeable membrane. As the reaction proceeds forward, hydrogen is selectively removed and exits in a separate stream at low pressure.

2.1 Advantages of Membrane Reactors

The stated advantages of membrane reactors, which are the same for all membrane reactor applications, will be illustrated in the following example of the steam reforming of methane.

2.1.1 Steam-Methane Reforming

The overall reaction for the steam reforming of methane is as follows:

$$CH_4 + 2H_2O \rightarrow 4H_2 + CO_2. \tag{2.1}$$

This reaction can be modeled as occurring in two stages [12]. The first involves the endothermic, irreversible cracking of methane:

$$CH_4 + H_2O \rightarrow 3H_2 + CO \quad \Delta H_r^\circ = 164.6\text{kJ/mol}CH_4 \tag{2.2}$$

followed by the water-gas shift:

$$CO + H_2O \longleftrightarrow CO_2 + H_2 \quad \Delta H_r^\circ = -41.2\text{kJ/mol}CO \tag{2.3}$$

which is exothermic and equilibrium-limited. It is preferred that reaction (2.2) be performed at high temperature and pressure because reaction rates are higher and catalyst use is improved under these conditions [12]. This reaction is highly endothermic, which means that the entrance temperature must be high and heat must be provided along the length of this portion of the reactor. By contrast, reaction (2.3) is exothermic and the extent of the reaction is greatest when it

occurs at low temperature and low pressure. Therefore, heat must be removed either between this stage and the last or along this portion of the reactor. Because low pressures are needed to drive the shift reaction, both reactions are typically performed at low pressures (below 100 psi). The result is a much larger reactor than would be required if high pressure cracking were performed. The large size increases equipment costs and exacerbates the complicated heat transfer process. Moreover, the CO content in the stream after the water-gas shift is still too high: 1-2%. Polymer electrolyte membrane (PEM) fuel cells and other low temperature fuel cells are poisoned by these high concentrations of CO, making some post-shift "clean-up" necessary. PEM fuel cells require CO levels between 10 and 20 parts per million, and would operate more efficiently with even lower CO content levels. Amphlett et al. have shown that the power density of this fuel cell would be three times greater, that is, PEM cells would be one-third their size, if the hydrogen source were perfectly pure. Partial combustion after the shift can be used to reduce CO content levels sufficiently, but the catalyst required for the process consumes hydrogen. In addition to producing purer output hydrogen, membrane reactors can obviate the low pressure purification process by fundamentally improving the dependence of the extent of the reaction on pressure. This will be demonstrated in the following example.

In a thought experiment, we write an equilibrium constant for the overall reaction (2.1), expressed first in terms of the partial pressures of the various species and then in terms of their mole fractions and the total pressure of the gas mixture:

$$K_C = \frac{P_{H2}^4 P_{CO_2}}{P_{H_2O}^2 P_{CH_4}} = P_{Tot}^2 \frac{y_{H_2}^4 y_{CO_2}}{y_{H_2O}^2 y_{CH_4}} \tag{2.4}$$

where K_C is the concentration-based equilibrium constant, P_i is the partial pressure of species i, P_{Tot} is the total pressure, and y_i is the mole fraction of component i. $y_i = P_i/P_{Tot}$. If reaction (2.1) were to go to completion in a traditional (non-membrane) reactor, then one mole of methane and two moles of water would yield four moles of hydrogen and one mole of carbon dioxide. For a reaction that is not driven to completion, we define the extent of the reaction β to be the number of moles of carbon dioxide produced. The number of moles of hydrogen is then 4β, the moles remaining of methane and water are then $1-\beta$ and $2-2\beta$ respectively, and the total number of moles in the system must be $3+2\beta$. Substituting into the rightmost expression in equation (2.4),

we obtain

$$\frac{K}{P_{Tot}^2} = \frac{\beta(4\beta)^4}{(1-\beta)(2-2\beta)^2} \frac{1}{(3+2\beta)^2} \tag{2.5}$$

Clearly lower pressures yield higher conversions in this case.

This relationship between extent of reaction β and total pressure in a traditional non-membrane reactor is illustrated in Figure 2.2.

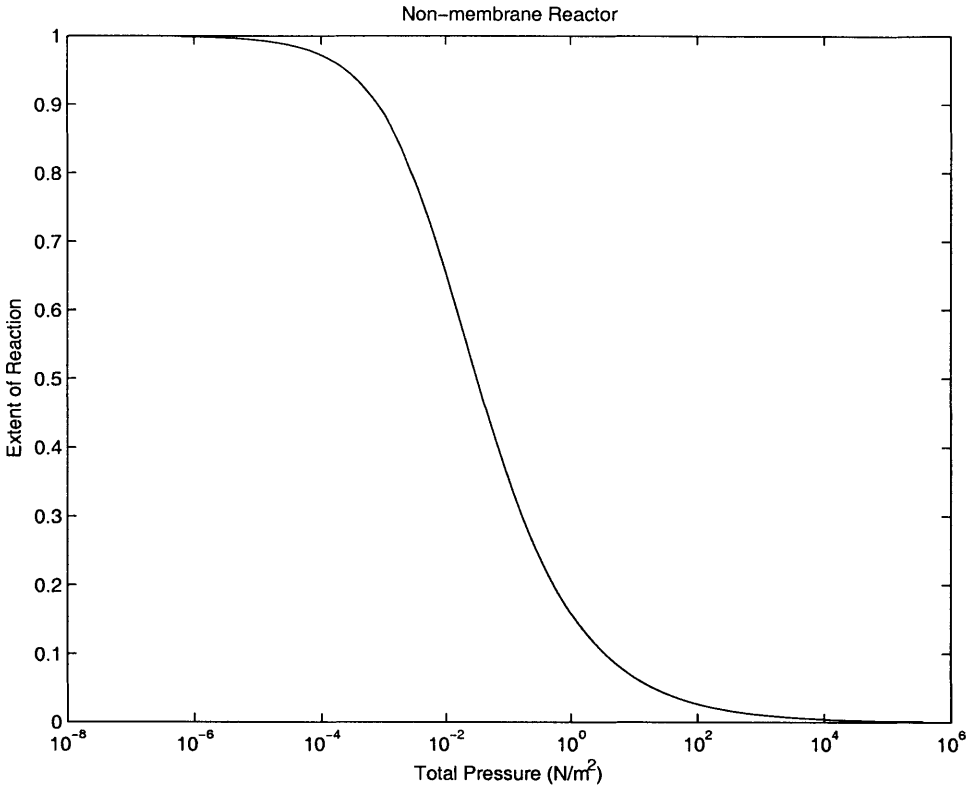

Figure 2.2: Illustration of the relationship between extent of reaction and total pressure in a non-membrane reactor.

In a membrane reactor in which hydrogen is selectively removed, such as the one sketched in Figure 2.3, equilibrium conditions are met only in the plane at the exit of the reactor. Prior to the exit plane, the reaction is presumably still proceeding forward. "P_{tot}" is then the total pressure of the gases in the core of the reactor in this exit plane only.

The partial pressure of hydrogen can be modeled as a function not only of the extent of reaction, but also of the back-pressure at the hydrogen outlet. (In an arbitrary mobile application, P_{back}

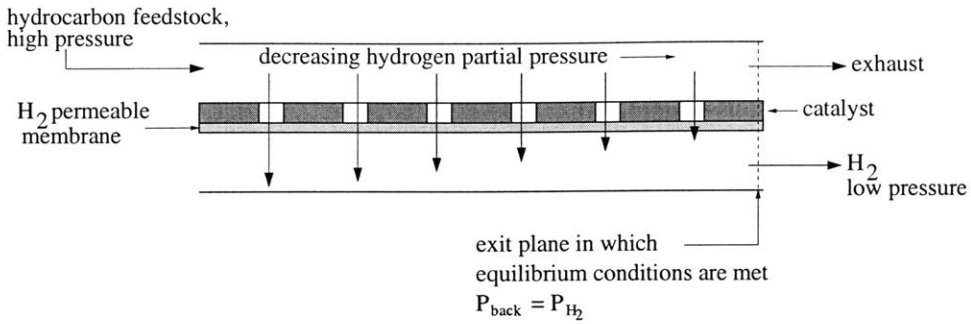

Figure 2.3: Illustration of where equilibrium conditions are expected in a membrane reactor.

could be approximately 1 atm.) According to the work by Lund, transport resistance through the membrane is non-negligible, but it is minimal, and so for the purposes of this example, $P_{H_2} = P_{back} = \text{const}$ [7]. The number of moles of H_2, CO_2, CH_4, and H_2O present in the exit plane are as follows:

$$n_{H_2} = \frac{P_{back}}{P_{tot} - P_{back}}(3 - 2\beta)$$

$$n_{CO_2} = \beta$$

$$n_{CH_4} = 1 - \beta$$

$$n_{H_2O} = 2 - 2\beta$$

and the total number of moles in the core of the reactor in the exit plane is

$$n_{total} = \frac{P_{tot}}{P_{tot} - P_{back}}(3 - 2\beta).$$

We now rewrite the right-most expression of equation (2.4) as

$$K_C = \frac{P_{back}^4}{P_{tot}^2} \frac{y_{CO_2}}{y_{CH_4} y_{H_2O}^2}. \tag{2.6}$$

Algebra yields

$$K_C \frac{P_{tot}^2}{P_{back}^4} = \frac{\beta}{(1-\beta)(2-2\beta)^2} \frac{P_{tot}^2(3-2\beta)^2}{(P_{tot}-P_{back})^2}$$

or

$$P_{tot}^2 - 2P_{tot}P_{back} + P_{back}^2 - \frac{P_{back}^4}{K_C} f(\beta) = 0$$

where

$$f(\beta) = \frac{9\beta - 12\beta^2 + 4\beta^3}{4(1-3\beta+3\beta^2-\beta^3)}.$$

This quadratic in P_{tot} is solved for variable P_{back} and a family of curves illustrating the relationship between the total pressure and extent of reaction are plotted in Figure 2.4. In this figure it can be seen that, very unlike the non-membrane reactor case, increasing the total pressure of the gas mixture increases the extent of reaction. Furthermore, the extent of reaction in a membrane reactor can be further increased by decreasing the back pressure at the hydrogen exit.

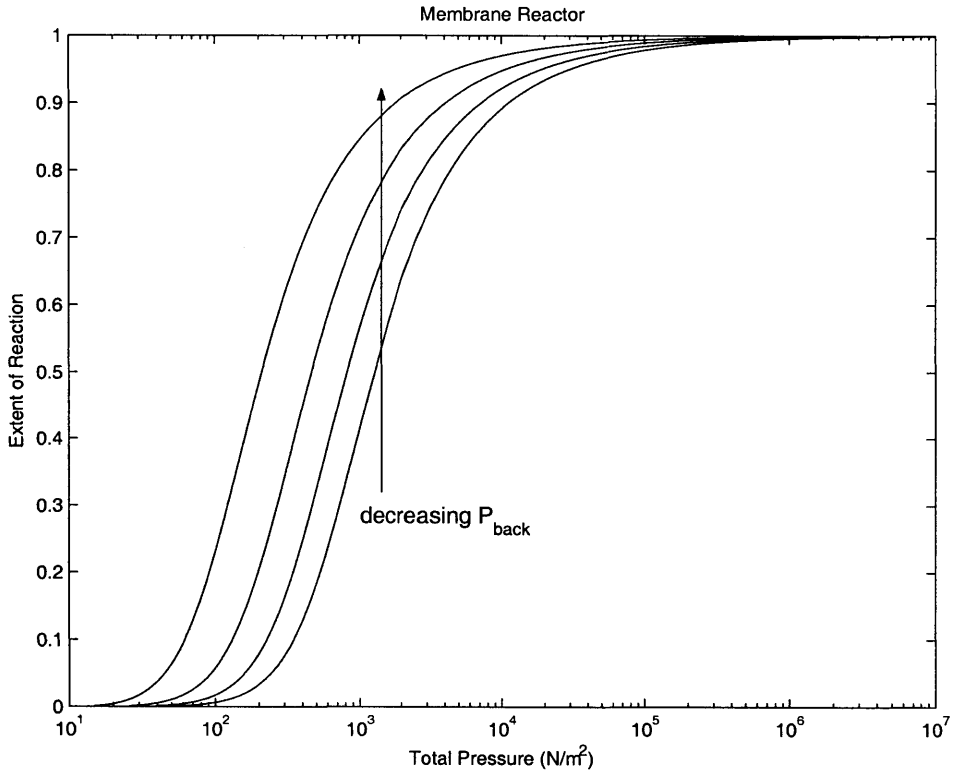

Figure 2.4: Dependence on pressure of the extent of reaction in a membrane reactor.

The fact that higher pressures yield greater conversions allows significant design improvements

and is a fundamental advantage of membrane reactors. Additionally, since volumetric flow rate for gases decreases inversely with total pressure at a given molar flow rate, $P\dot{V} = \dot{m}RT$, the higher pressures in a membrane reactor decrease the volumetric flow rate for a given mass flow rate of gas. More importantly, the higher pressures and subsequent smaller volume flow rates increase the residence time of the reactants for a given size of reactor. This means that less catalyst and thus a smaller reactor could be used for a given mass flow rate of gas. In order to benefit from these fundamental advantages of membrane reactors, a good catalyst for a given operating temperature range must be identified and a membrane strong enough to withstand the pressure differential $P_{tot} - P_{back}$ must be found.

Chapter 3

The Current Work

It was noted in the example of the previous chapter that, in regard to energy related issues, the water-gas shift is part of the process of reforming hydrocarbons to produce hydrogen suitable for fuel cells. Carbon monoxide poisons the low temperature fuel cells and must therefore be removed. The water-gas shift, a reaction in which CO is consumed and H_2 is produced, is thus a focal point in the development of improved fuel reforming processes. The reaction is also a focal point in the development of membrane reactors because improving reactors for the shift can result in an even greater improvement in the economy of steam and thus overall system efficiency in fuel reforming plants.

3.1 The Water-Gas Shift

The reaction is limited by thermodynamic equilibrium at the higher temperatures while kinetics are unfavorable at the lower temperatures. Below is an expression for the equilibrium constant for this reversible and exothermic reaction; Figure 3.1 illustrates how strongly K_C varies with temperature.

$$CO + H_2O \longleftrightarrow CO_2 + H_2 \qquad \Delta H^0 = -41.2\text{kJ/mol CO} \tag{3.1}$$

$$K_p = \frac{103943}{\exp\left[\frac{41147.4}{R}\left(\frac{1}{T} - \frac{1}{298}\right)\right]} \tag{3.2}$$

where R is the universal gas constant, 8.314J/mol·K.

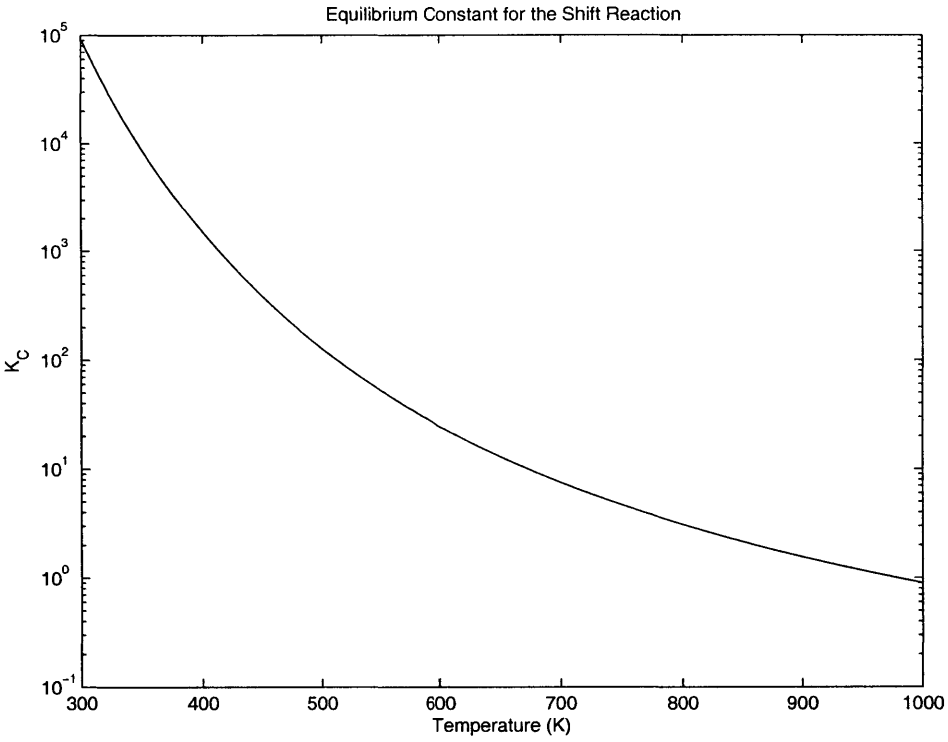

Figure 3.1: Dependence of the equilibrium constant for the water-gas shift reaction on temperature.

Catalysis is extremely important in the case of such exothermic, equilibrium-limited reactions. Higher temperatures are required to make the reaction occur, but an appropriate catalyst for a given reaction can improve kinetics even at the lower temperatures. In the case of the water-gas shift, the effects of equilibrium limitations are greatest at the higher temperatures and excess steam is often used to improve CO conversions at these higher temperatures. Table 3.1 summarizes how much excess steam would be required for a theoretical 100% conversion of CO at various temperatures.

Operating Temperature, K	Steam Requirement in Single-Stage Reactor, ft^3/ft^3 CO
623	6.98
728	22.3
828	50.3

Table 3.1: Steam requirements for theoretical conversion in the shift reaction (Sherwood, 1961).

3.2 Current Means of Catalyzing the Shift

In Figure 1.1, two separate adiabatic beds are used to catalyze the water-gas shift as part of the purification stages of H_2 production via steam methane reforming. The two separate catalytic reactors address the trade-off between fast kinetics and high equilibrium conversions of CO. The first bed is a high temperature bed in which kinetics are fast, but overall equilibrium conversions are lower than they need to be. The catalyst in this first bed is an industry standard made of Fe_3O_4 with a Cr_2O_3 promoter. The operating range of the ferro-chrome catalyst is between 600K and 750K. At 750K, where kinetics are most favorable, over $22m^3$ of steam per m^3 of CO would be theoretically required to overcome the equilibrium limitation. Instead of adding this much excess steam to the feed stream, a second, lower temperature bed is employed to achieve sufficiently high overall conversions. A copper based catalyst is used in this second bed. Any CO remaining in the stream after this second stage of the water-gas shift must be separated out, which is often done with a pressure swing adsorption system at low pressure. The fact that the pressure swing adsorption system requires low pressures is inherently problematic for a steam reforming plant like the one shown in Figure 1.1. As discussed in Chapter 2, the cracking of methane is most efficient

at high pressures. The traditional water-gas shift reactors are most efficient at lower pressures, and the pressure swing adsorption system requires near vacuum pressures. Maintaining these extreme pressure differentials would require extensive adjunct machinery; instead, the whole system is often run near isobarically, at low pressure, at a sacrifice to the plant efficiency. A great improvement would be to catalyze the shift at high temperatures and pressures, and to separate the H_2 out of the stream concurrently, obviating the pressure swing adsorption system.

3.3 Future Plans for Catalyzing the Shift

Membrane reactors are currently being tried for their potential benefits in a water-gas shift reactor application. They would eliminate the thermodynamics/kinetics trade-off by separating either the hydrogen or the carbon dioxide while the forward reaction is in progress. Today, the development of membrane reactors for the shift is deeply tied to the development of suitable catalysts. The thermodynamic and chemical environment in a membrane reactor is vastly different from the environment in a traditional reactor. The pressures are higher and the feed is closer to stoichiometric as significantly less excess steam is required. The amount of excess steam required is now a function of the maximum adiabatic temperature that the catalyst can withstand; a higher temperature catalyst is thus preferred not only because the kinetics are faster at higher temperatures but also because it allows for the minimal use of excess steam. Traditional shift catalysts are not well studied under the conditions of high temperature, high pressure and minimal excess steam. In 1969, Bohlbro presented an extensive study of the shift reaction over ferro-chrome (Bohlbro, 1969). Very briefly, he experimentally found a rate expression for the reaction under a multitude of controlled conditions. He illustrated how an excess of carbon dioxide inhibits the forward reaction. In order for ferro-chrome to be used as the catalyst in a membrane shift reactor, it seems that it would be preferable to remove the inhibitor, CO_2. However, it was recently noted that selectively removing the CO_2, leaving the catalyst exposed to high concentrations of hydrogen, causes reduced and thus inactive forms of iron to appear in the catalyst effluent [7]. The ferro-chrome catalyst is thus dysfunctional in an environment of excess hydrogen or excess carbon dioxide. For these reasons, it is suspected that catalysts other than the industry standard catalysts for the traditional shift reactors are more suitable for the membrane application, and the development of such catalysts

is both deep and widespread. A cobalt-molybdenum catalyst, though not yet well-studied, shows promise.

3.4 The Proposed Work

The current work does not participate in this race for the best new shift catalyst possible for a membrane reactor, but, rather, creatively takes advantage of what is already known about ferro-chrome and the specific reasons why it is being disregarded for the membrane application. In a standard, non-membrane reactor, the concentrations of hydrogen and carbon dioxide are approximately the same and increasing as the reaction proceeds forward. This information suggests that ferro-chrome could be well suited for a membrane reactor that maintains concentrations of H_2 and CO_2 within a tolerable range for the catalyst at every cross section in the reactor; that is, perhaps it is the ratio of the two concentrations that must be well modulated in order for ferro-chrome to be fully functional. Modulating this ratio in a membrane reactor application for the shift requires that both hydrogen and carbon dioxide be removed, concurrently, from the core of the reactor. This is, essentially, the objective of the current work. Figure 3.2 is a schematic of the proposed reactor. There are currently no membrane shift reactors on the market like this one.

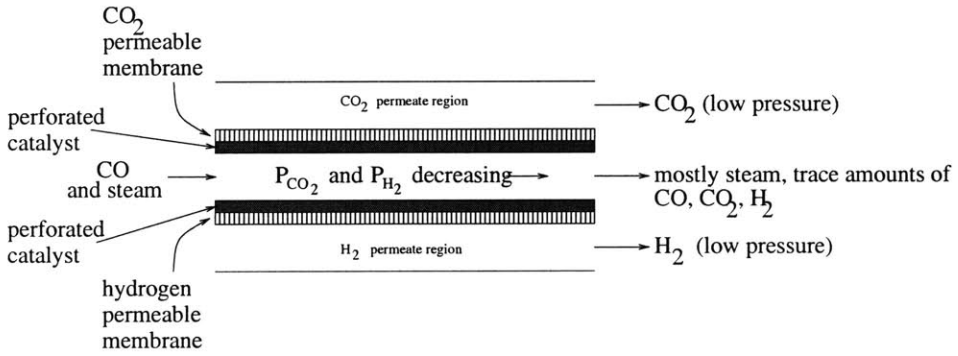

Figure 3.2: Schematic of the proposed membrane reactor for the water-gas shift. Carbon monoxide and steam enter the reactor at high pressure, react on the surface of a porous catalyst that is backed on one side by a H_2-selective membrane, and on the other side by a CO_2-selective membrane. These two products of the reaction exit the reactor in two separate, low-pressure streams; the exhaust consists primarily of steam with trace amounts of unreacted CO and trace amounts of the products.

3.4.1 Membranes

The membranes are a backing to the porous catalyst structure and separate the core of the reactor from the H_2 and CO_2 permeate regions of the reactor. Pressures in the core of the reactor are high whereas pressures in the permeate regions of the reactor are maintained low. While the reaction proceeds forward, these membranes selectively remove hydrogen on one side (the bottom side, as shown in the figure) and carbon dioxide on the other side. This design is, in a basic sense, two membrane reactors like the one shown in Figure 2.1 combined into one structure. The two product gases are driven out of the core of the reactor by the pressure differential across the membranes. The hydrogen-selective membrane will be a palladium derivative, an industry standard. The CO_2-selective membrane will be one of the following three available:

1. a thin film zeolite membrane that chemically selects CO_2, developed at Sandia National Laboratories [4].

2. a polyvinyl alcohol network with amines that actively transport CO_2 across the membrane [5].

3. a ceramic membrane that has demonstrated notable resistance to fouling developed at UCLA in conjunction with Media and Process Technology, Inc. [6].

Both membranes must be thin enough to minimize resistance to mass transport, but strong enough to withstand large pressure differentials. If lack of strength becomes an issue, the membranes will have to be appropriately reinforced (on the permeate side).

Another concern regarding the membranes is the effect of CO. CO is known to block the transport of H_2 through palladium-based membranes, and CO could potentially migrate through the CO_2-selective membranes. For these reasons, care must be taken to minimize the amount of CO that reaches the membrane. This will be achieved by making the porous catalyst layer appropriately thick, and with moderate amounts of excess steam to encourage the consumption of CO. If the forward reaction is favorable enough, and if the residence time of CO is short, it is expected that the amount of CO to reach the membrane will be minimal. In a paper by Karnik et. al, H_2 was successfully removed using a palladium-based membrane while the water gas shift proceeded over copper [17]. Our treatment of the H_2-selective membrane will be patterned after

this work.

The current work is in the early stages of modeling the thermochemistry and kinetics of the proposed duo-selecting membrane reactor. The next chapter describes these models in detail.

Chapter 4

The Thermodynamic Model

4.1 First and Second Laws of Thermodynamics

Below is a sketch of the reactor viewed, from a thermodynamic sense, as a "black box" into which carbon monoxide and steam go in, and three steams come out: unreacted CO and steam, hydrogen, and carbon dioxide.

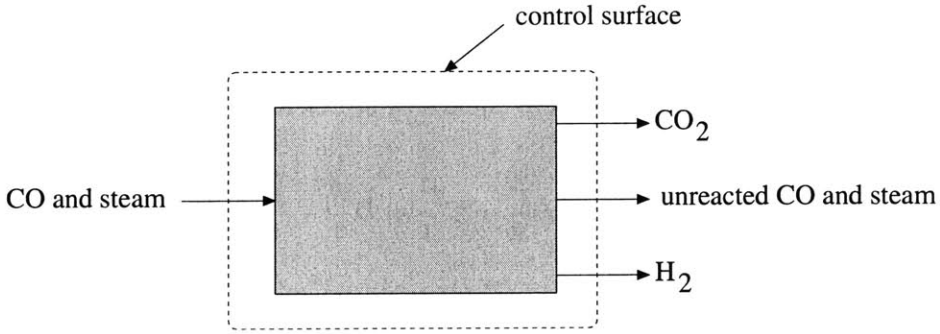

Figure 4.1: Set-up for the thermodynamic model.

The first and second laws of thermodynamics for the steady-state control volume shown are as follows:

$$Q - W = H_{out} - H_{in} \tag{4.1}$$

$$S_{gen} = S_{out} - S_{in} - \frac{Q}{T_{gas}} > 0 \tag{4.2}$$

$W = 0$, and the incomplete reaction with appropriate stoichiometric coefficients is

$$CO + \eta H_2O \longleftrightarrow \beta CO_2 + \beta H_2 + (\eta - \beta)H_2O + (1 - \beta)CO \tag{4.3}$$

η is the steam to gas ratio; that is, η is the number of moles of steam that are added per mole of CO. β is the extent of reaction, defined as the number of moles of CO_2 produced. The number of moles of H_2 and CO_2 are assumed to be equal in this model; that is, the extent of reaction is also the number of moles of hydrogen produced.

The first and second laws are now rewritten as the following:

$$Q = [\beta h_{H_2} + \beta h_{CO_2} + (\eta - \beta)h_{H2O} + (1 - \beta)h_{CO}]_{exit} - [\eta h_{H2O} + h_{CO}]_{in} \tag{4.4}$$

$$S_{gen} = [\beta s_{H_2} + \beta s_{CO_2} + (\eta - \beta)s_{H2O} + (1 - \beta)s_{CO}]_{exit} - [\eta s_{H2O} + s_{CO}]_{in} - \frac{Q}{T_{gas}} > 0 \tag{4.5}$$

The enthalpies and entropies for the various species are approximated using the coefficients for the Shomate Equation provided in the National Institute for Science and Technology's online Chemistry Webbook[1]. For $t = T(K)/1000$, the Shomate equations are as follows:

$$h^\circ - h^\circ_{298K} = At + B\frac{t^2}{2} + C\frac{t^3}{3} + D\frac{t^4}{4} - \frac{E}{t} + F - H \tag{4.6}$$

$$s^\circ = A\ln(t) + Bt + C\frac{t^2}{2} + D\frac{t^3}{3} - \frac{E}{2t^2} + G \tag{4.7}$$

The coefficients for the Shomate equations are tabulated below.

The Shomate approximation for the entropy of a species gives the temperature dependent contribution to the entropy. The pressure dependent contribution must be added as $-R\ln(P_i/P_{atm}) + s^\circ_{1bar}$. The first of these two terms must be calculated from the mole fraction of the species, but the second term is a constant. The values of this constant for the four species of interest are tabulated in column "I" of the table.

[1]http://webbook.nist.gov/chemistry

	A	B	C	D	E	F	G	H	I
H_2	33.07	-11.36	11.43	-2.77	-0.16	-9.98	172.71	0.00	130.68
CO_2	25.00	55.19	-33.69	7.95	-0.14	-403.61	228.24	-393.52	213.78
H_2O	30.09	6.83	6.79	-2.53	0.08	-250.88	223.40	-241.83	188.84
CO	25.57	6.10	4.05	-2.67	0.13	-118.01	227.37	-110.53	197.66

Table 4.1: Coefficients for the Shomate equations (NIST website).

In this thermodynamic model, the reactor is assumed to operate isobarically. The optimal operating pressure will have to be determined from a study of the kinetics of the reaction, but for now the pressure in the core of the reactor is assumed to be six atmospheres.

4.2 Isothermal Mode of Operation

These laws are used to predict the extent of reaction β in the two cases of isothermal and adiabatic operation. In the isothermal case, the upper bound of the extent of reaction is predicted from the equilibrium constant for a given temperature T(K) and steam:gas ratio, η:

$$K_C = \frac{y_{H_2} y_{CO_2}}{y_{H_2O} y_{CO}} = \frac{\beta^2}{(\eta - \beta)(1 - \beta)} = \frac{103943}{\exp\left[\frac{41147.4}{R}\left(\frac{1}{T} - \frac{1}{298}\right)\right]} \tag{4.8}$$

where R is the universal gas constant, 8.314J/mol·K. Only temperatures between 660K and 750K are considered, since this is the operating range of the catalyst. Figure 4.2 shows the relationship between η and β for the isothermal case. This figure shows that, at $P = 6$ atm, a minimum amount of steam is required to meet the equilibrium limitation of the reaction. For too little steam, the second law of thermodynamics is satisfied only for smaller values of the extent of reaction. Following the plot of β versus η for this isothermal case are plots illustrating the relationship between S_{gen} and η, and ΔH and η. The Matlab scripts that generate the data for these plots are included in the appendix.

4.3 Adiabatic Mode of Operation

In the adiabatic case, the following conditions must be met:

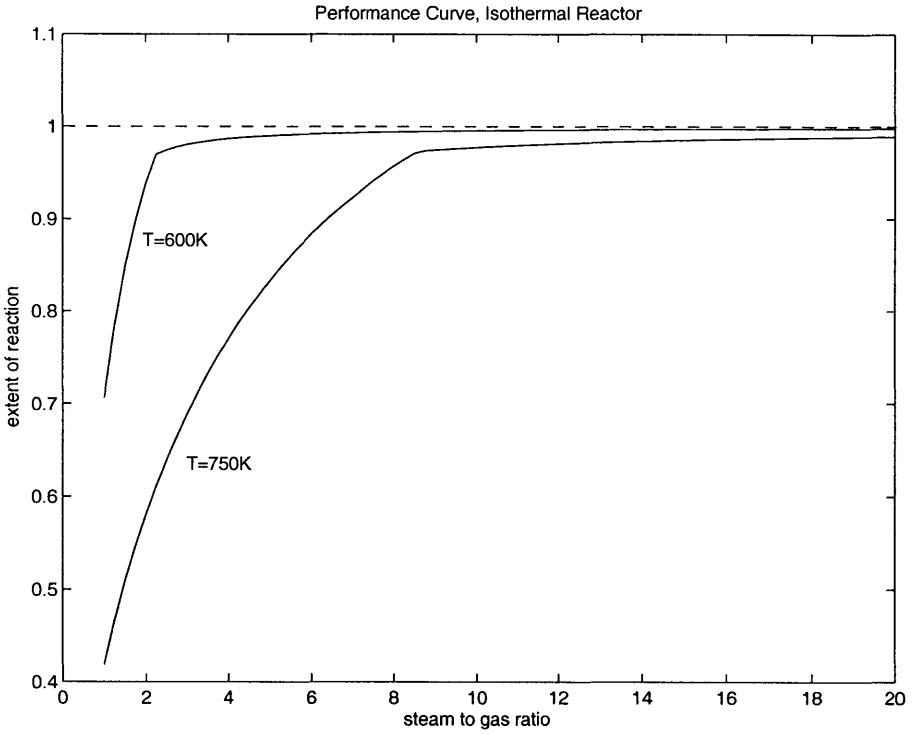

Figure 4.2: Illustration of the relationship between η and β for the isothermal case. As expected, equilibrium conversions are highest at the lower temperatures.

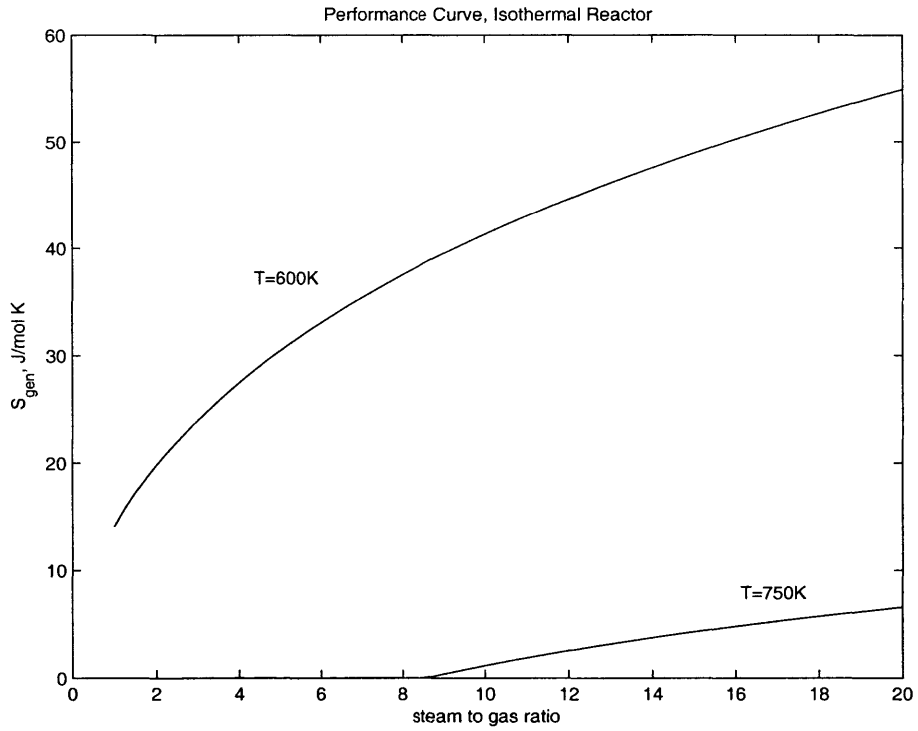

Figure 4.3: The second law limit on the extent of reaction in the isothermal case when η is too low.

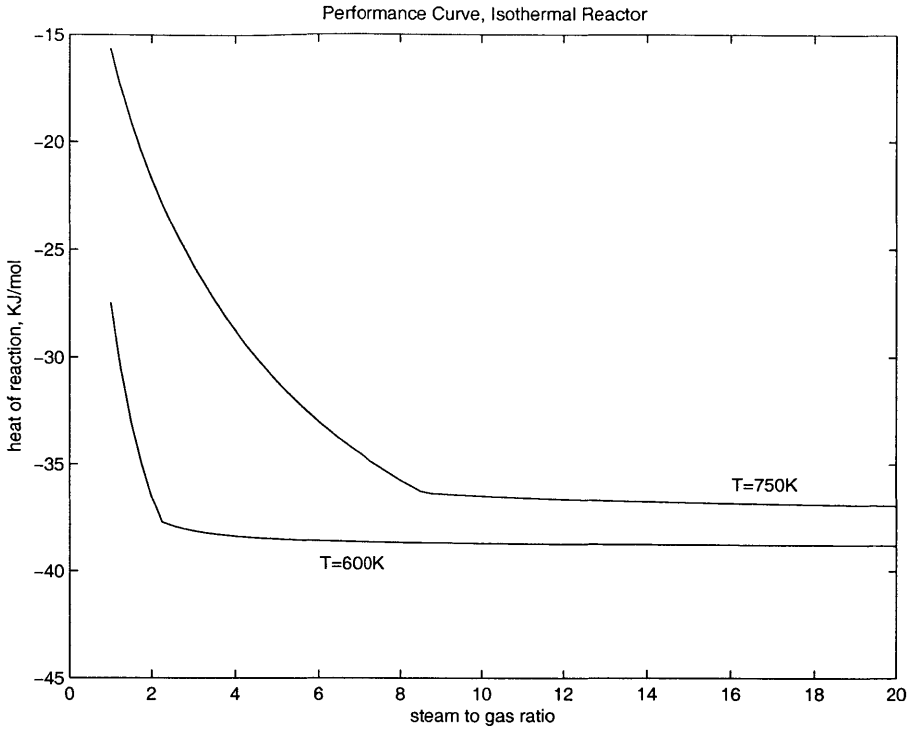

Figure 4.4: The heat transfer out of the system necessary to maintain isothermal conditions.

1. $\Delta H = 0$, and

2. $S_{gen} \geq 0$.

Another Matlab script, also included in Appendix A, was written to determine the extent of reaction iteratively in this adiabatic case. The highest possible value of β attainable for a given flame temperature is $\beta(T_{out})$, where T_{out} is the temperature of the mixture upon exiting the reactor. Therefore, $\beta_{adiabatic} \leq \beta(T_{out})$. The Matlab script, adiabatic.m, tries this maximum value first to check if the value satisfies the two conditions. If $\beta(T_{out})$ is too high, a slightly lower value is tried, and the process repeats until the $\beta_{adiabatic}$ that satisfies the two conditions is obtained[2].

The relationship between η and $\beta_{adiabatic}$ is added to the performance curves for the isothermal cases and shown in Figure 4.5. A fourth curve representing $\beta(T_{out})$ is also shown in this plot. The up and down nature of the adiabatic curve is, in large part, attributed to the fact that the constraint on the first law ($\Delta H = 0$) is relaxed to allow for a reasonable computation time. The

[2]The results of the code were checked against the results of from Equil, a Chemkin program.

script adiabatic.m requires $|\Delta H| < 1$ J/mol.

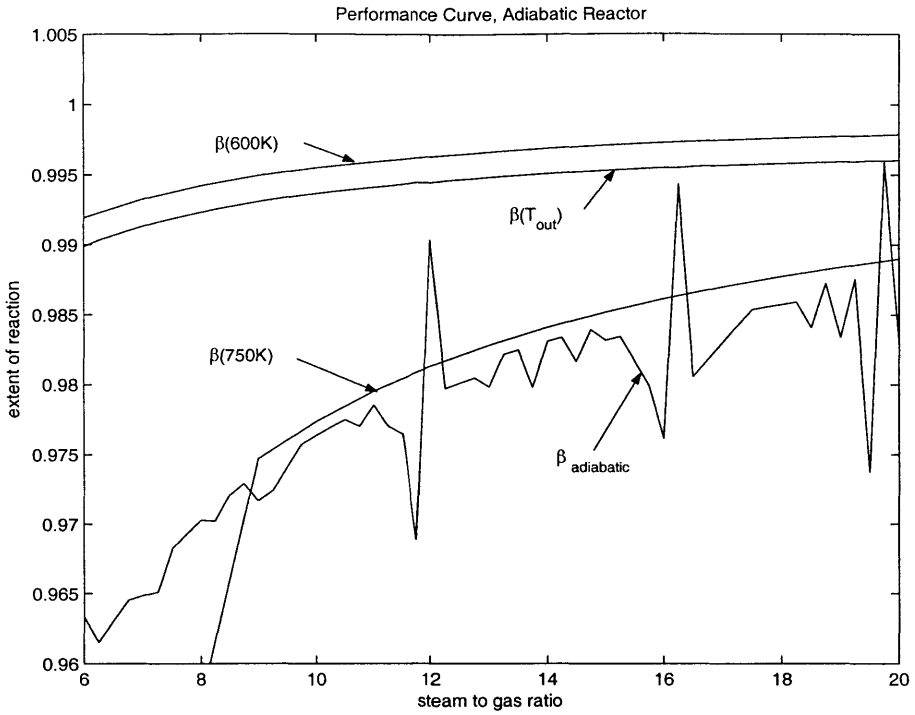

Figure 4.5: Comparison of the extents of reaction in the two isothermal cases ($T = 600$ K and $T = 750$ K), the adiabatic case, and the limiting adiabatic case when the extent of reaction is determined from the equilibrium constant at the flame temperature.

Following Figure 4.5 is a plot comparing the amounts of entropy generated in the two isothermal cases and the adiabatic case. While $T = 600$ K yields the greatest extent of reaction for a given value of η, this mode of operation also generates the most entropy. In this work, however, entropy generation does not weigh heavily in the recommendation for the choice of reactor operating conditions; the recommendation is based solely on hydrogen yield.

In Figures 4.5 and 4.6, steam to gas ratios less than 6 are not considered. This is because lower values of η result in a flame temperature above 750 K, which is the highest operating temperature of the catalyst. Figure 4.7 illustrates how the flame temperature varies with the steam to gas ratio.

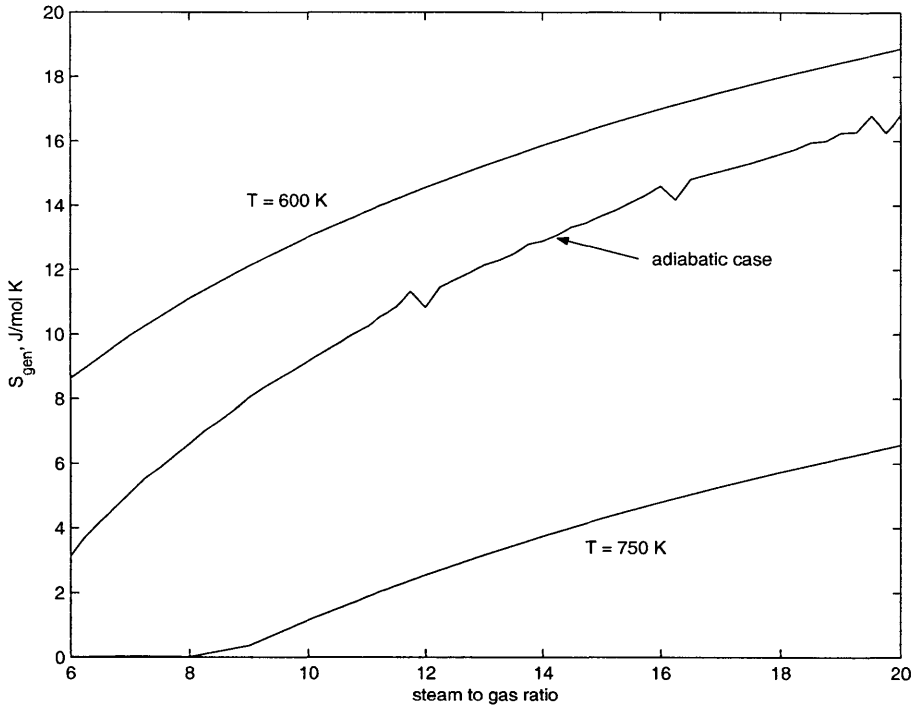

Figure 4.6: Comparison of entropy generation in the two isothermal cases ($T = 600$ K and $T = 750$ K) and the adiabatic case.

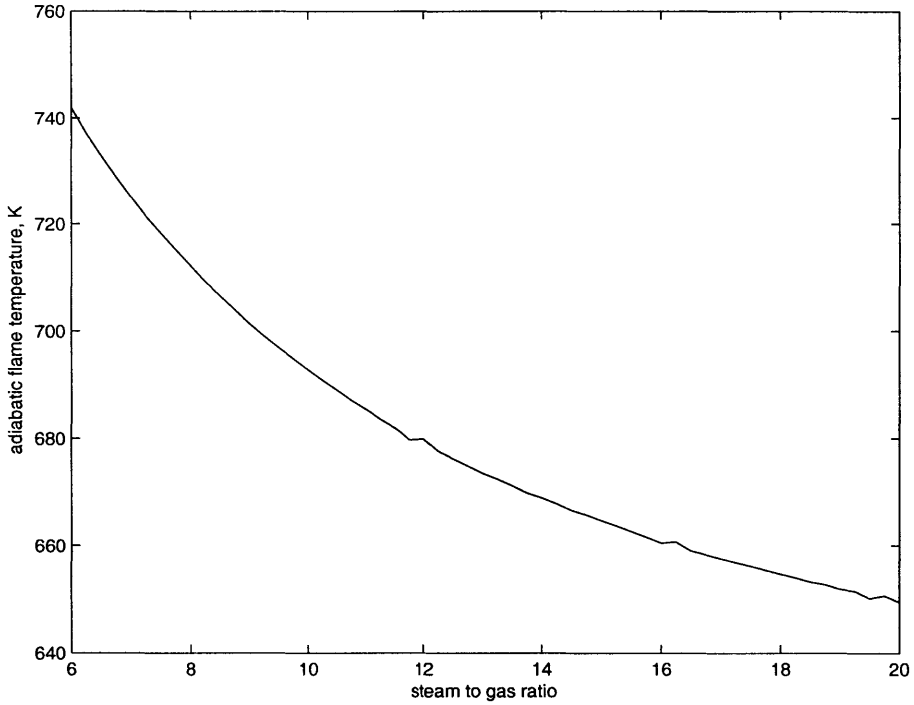

Figure 4.7: Dependence of the flame temperature on η for $\eta > \eta_{min} \approx 6$

Chapter 5

The Kinetic Model

5.1 Fundamentals of Equilibrium

The final equilibrium conversions, estimated in the thermodynamic modeling of the last section for adiabatic and isothermal operating conditions, does not lend insight into how much time is required in order for these conversions to be realized. The equilibrium constant, though used casually in previous examples, will be discussed in greater detail here. The equilibrium constant links thermodynamics to kinetics. The discussion begins with definitions of equilibrium.

The combined statement of the first and second laws of thermodynamics for a control mass undergoing an arbitrary quasi-static process is

$$TdS_{gen} = TdS - dU - pdV \geq 0. \tag{5.1}$$

The entropy generation must be positive, as stated originally in the second law, but at equilibrium, the entropy generation reaches a maximum. That is, when $dS_{gen} = 0$, it could only be because S_{gen} is a maximal value, which occurs only at equilibrium. Should the system be constrained by internal energy and volume, $dU = dV = 0$, this statement reduces to $dS \geq 0$. That is, entropy can only be maximized at constant (U, V) and is maximal at the equilibrium state. The definition of enthalpy can be used to change coordinates from (U, V) to (H, P): $H = U + PV$ and

$$TdS_{gen} = TdS - dH - VdP \geq 0. \tag{5.2}$$

This statement repeats that the entropy generation is maximized at equilibrium, regardless of what external constraints might be placed on the system. If the system is constrained by enthalpy and pressure, then $dS \geq 0$ and the entropy is also maximized at equilibrium.

The definition of the Gibbs free energy, $G = H - TS$, yields a second change of coordinates.

$$TdS_{gen} = -dG - VdP - SdT \geq 0. \tag{5.3}$$

If the system is constrained to constant temperature and pressure, then $dG \leq 0$, which states that the Gibbs free energy is minimized at the equilibrium state.

Equation 5.4 is Gibbs' Fundamental Equation of thermodynamics applied to a control mass.

$$TdS = dU + PdV \tag{5.4}$$

Gibbs' Equation is the combined statement of the first and second laws of thermodynamics for a reversible process in which $\delta Q = TdS$ and $S_{gen} = 0$. In this equation, S is a function of the two independent variables, U and V. $S = S(U, V)$. Differentiating this expression using the chain rule,

$$dS = \left(\frac{\partial S}{\partial U}\right)_V dU + \left(\frac{\partial S}{\partial V}\right)_U dV. \tag{5.5}$$

This expression, combined with Equation 5.4 yields the following:

$$\frac{1}{T} = \left(\frac{\partial S}{\partial U}\right)_V \tag{5.6}$$

and

$$P = T\left(\frac{\partial S}{\partial V}\right)_U \tag{5.7}$$

which are the fundamental definitions of temperature and pressure, respectively.

For a mixture of different chemical species, Gibbs' Fundamental relation is extended to reflect the contribution of the various species to the total entropy:

$$TdS = dU + PdV - \sum_N \mu_1 dn_i. \tag{5.8}$$

n_i is the the number of moles of species i and μ_i is the chemical potential of species i. The entropy is now a function of the number of moles of each species in addition to the internal energy and volume: $S = S(U, V, n_i)$. Differentiating this expression using the chain rule, we obtain:

$$dS = \left(\frac{\partial S}{\partial U}\right)_V dU + \left(\frac{\partial S}{\partial V}\right)_U dV + \sum_N \left(\frac{\partial S}{\partial n_j}\right)_{V,n_{i\neq j}} dn_j. \tag{5.9}$$

The chemical potential can now be defined as

$$\mu_i = -T\left(\frac{\partial S}{\partial n_i}\right)_{U,V,n_{j\neq i}}. \tag{5.10}$$

Gibbs' Fundamental Equation can be rewritten in energy terms as

$$dU = TdS - PdV + \sum_N \mu_i dn_i \tag{5.11}$$

so that $U = U(S, V, n_i)$. Following a similar procedure as before, we obtain another definition of chemical potential:

$$\mu_i = \left(\frac{\partial U}{\partial n_i}\right)_{S,V,n_{j\neq i}}. \tag{5.12}$$

Substituting the definitions of the enthalpy and Gibbs free energy into Gibbs' Equation yield two more definitions of chemical potential:

$$\mu_i = \left(\frac{\partial H}{\partial n_i}\right)_{S,P,n_{j\neq i}}, \text{and} \tag{5.13}$$

$$\mu_i = \left(\frac{\partial G}{\partial n_i}\right)_{T,P,n_{j\neq i}}. \tag{5.14}$$

A more practical definition of chemical potential can be obtained by noting that, in a mixture of chemical species, a system property is the sum of each species' contribution. For example, $S = \sum_N n_i \hat{s}_i$. If we write $dn_i = n_i d\epsilon$ to linearize the change in a system property, then

$$dS = d\left(\sum_N dn_i \hat{s}_i\right) = \left(\sum_N n_i \hat{s}_i\right) d\epsilon = S d\epsilon. \tag{5.15}$$

Similarly, we can show that $dU = U d\epsilon$ and $dV = V d\epsilon$. Gibbs' Fundamental Equation (in terms of

energy) is then

$$U = TS - PV + \sum_N \mu_i n_i. \tag{5.16}$$

Since $H = U + PV$,

$$H = TS + \sum_N \mu_i n_i.$$

The expression is further simplified by the definition of Gibbs free energy, $G = H - TS$:

$$G = \sum_N \mu_i n_i. \tag{5.17}$$

This last result allows us to calculate the chemical potential of a species in a mixture as the molar Gibbs free energy of that species at a given temperature and partial pressure:

$$\mu_i = \hat{g}_i(T, P_i) = \hat{h}_i - T\hat{s}_i(T, P_i) \tag{5.18}$$

where, in a mixture of ideal gases, the entropy is calculated at the partial pressure of a given species. The Gibbs free energy can then be written as

$$\hat{g}_i^o(T) + RT \ln \frac{P_i}{P_o} \tag{5.19}$$

where $\hat{g}_i^o(T)$ is evaluated at 1 atmosphere and is a function of temperature only. When calculating the change in Gibbs free energy of a reaction, the stoichiometric coefficients ν_i are required. ΔG_r is then expressed as

$$\Delta G_r = \sum_{prod} \nu_i \hat{g}_i(T, P_i) - \sum_{reac} \nu_i \hat{g}_i(T, P_i) = \sum_{prod} \nu_i \hat{g}_i^o(T) - \sum_{reac} \nu_i \hat{g}_i^o(T) + RT \ln \frac{\prod_{prod} P_i^{\nu_i}}{\prod_{reac} P_i^{\nu_i}} \tag{5.20}$$

where all partial pressures are now written in terms of atmospheres. At equilibrium, $\Delta G_r = 0$. Rearranging,

$$\exp\left(-\frac{\Delta G_r^o(T)}{RT}\right) = \frac{\prod_{prod} P_i^{\nu_i}}{\prod_{reac} P_i^{\nu_i}} \equiv K_p(T). \tag{5.21}$$

This last relationship defines the equilibrium constant. Writing $\Delta G_r^o(T) = \Delta H_r(T) - T\Delta S_r(T)$

allows us to express the equilibrium constant in terms of the heat of reaction, as follows:

$$K_p(T) = \exp\left(-\frac{\Delta H_r(T)}{RT}\right)\exp\left(\frac{\Delta S_r(T)}{R}\right). \tag{5.22}$$

Taking the natural logarithm of both sides and differentiating yields the van't Hoff Equation:

$$\frac{d\ln K_p}{d\left(\frac{1}{T}\right)} = -\frac{\Delta H_r}{R}. \tag{5.23}$$

The slope of the $\ln K_p$ versus $1/T$ curve is minus the heat of reaction divided by the universal gas constant. This plot is shown in Figure 5.1 for the water-gas shift.

$$K_p = \frac{103943}{\exp\left[\frac{41147.4}{R}\left(\frac{1}{T} - \frac{1}{298}\right)\right]} \tag{5.24}$$

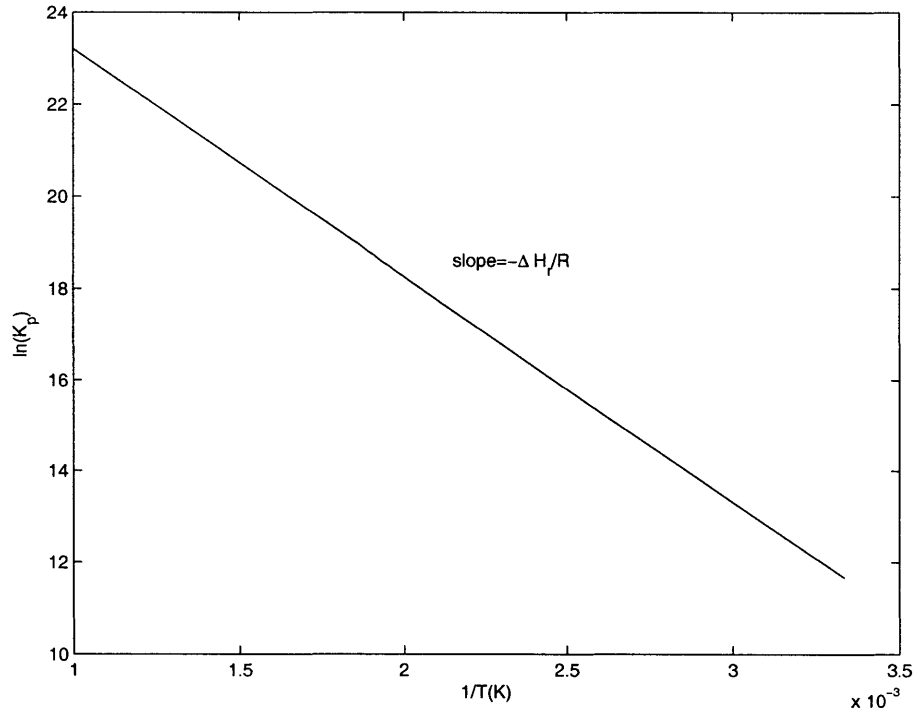

Figure 5.1: Illustration of the linear relationship between $\ln K_p$ and $1/T$.

Equilibrium states are reached asymptotically, not instantaneously. For this reason, especially in consideration of chemical reactor development, the kinetics of a reaction are at least as important

as the final equilibrium state.

5.2 Gas-Phase Kinetics

Chemical reactions are either homogeneous or heterogeneous, depending on whether a single phase or multiple phases participate in the reaction. The behavior of homogeneous gas-phase chemistry is more predictable, while the behavior of heterogeneous reactions, especially when surface chemistry is involved, must be observed in experimentation. The future of the current work is heavily centered around experimentation that will determine the behavior of the water-gas shift reaction over a ferrochrome surface when both products of the reaction are removed *in situ*. Details describing those plans are included in the chapter regarding Future Work. Presently, the gas-phase chemistry of the water-gas shift is studied in order to create a framework in which to proceed with the more complex, more realistic problem.

In what follows, the kinetics of a gas-phase reaction will be discussed in general, beginning with the description of elementary reactions and then proceeding to describe how to quantify the rate of an elementary reaction. The discussion will conclude with an example specific to the water-gas shift reaction.

5.2.1 Elementary Reactions

An elementary reaction is a reaction in which only a single bond is either broken or formed. Most homogeneous elementary reactions involve collision between molecules in which kinetic energy is transformed into chemical bond energy (or vice versa). There are three types of elementary reactions: decomposition, radical, and recombination. In a decomposition reaction, a molecule (AB) collides with a third body (M) and breaks into smaller fragments as follows:

$$AB + M \rightarrow A\cdot + B\cdot + M.$$

The third body provides the kinetic energy required for the dissociation but does not participate chemically in the reaction. $A\cdot$ and $B\cdot$ are radicals with a strong affinity to react with either another radical or a stable species.

A radical reaction involves at least one radical and can be written in generic form as:

$$AB + C\cdot \rightarrow A\cdot + BC. \tag{5.25}$$

If a radical reaction results in the same number of radicals on both sides of the chemical equation, the reaction is termed "chain propagating" or "shuffling." If the number of radicals increases as a result of the reaction, the reaction is termed "chain branching."

A recombination reaction is exactly the opposite of a decomposition reaction and can be written in generic form as:

$$A\cdot + B\cdot + M \rightarrow AB + M \tag{5.26}$$

where the third body M now carries away the equivalent chemical bond energy rather than provide it.

At respective rates depending on the temperature, pressure, and concentration of the various species participating in an elementary reaction, the reaction can proceed in either direction. The overall rate of a reversible reaction will be discussed after the rate of the forward reaction is expressed quantitatively.

For the two body reaction in the following chemical equation:

$$A + B \rightarrow C + D \tag{5.27}$$

the forward reaction rate can be expressed as

$$R_r = P_r Z_{AB} \exp\left(-\frac{\hat{E}_a}{RT}\right). \tag{5.28}$$

In this equation,

R_r is the rate of reaction defined as the rate of formation of either C or D;

P_r is the steric factor, determining the probability of collision based on orientation;

Z_{AB} is the collision frequency between molecules A and B;

$\hat{E}_a$ is the "activation" energy required for the reaction to proceed;

R is the universal gas constant;

T is the absolute temperature.

The collision frequency is given by

$$Z_{AB} = d_{AB}^2 \sqrt{\frac{8\pi N_b T}{m_{AB}}} n_a n_B. \tag{5.29}$$

In this expression,

d_{AB} is the collision diameter of molecules A and B;

N_b is the Boltzmann constant;

m_{AB} is given by $m_A m_B/(m_A + m_B)$;

n_i is the number of molecules per unit volume.

Dividing both sides of Equation 5.28 by Avogadro's number, the number of molecules per mole, we obtain the reaction rate in terms of moles per unit volume per second:

$$R_r = \left(P_r N_a d_{AB}^2 \sqrt{\frac{8\pi N_b}{m_{AB}}} \right) \sqrt{T}[A][B] = k(T)[A][B] \tag{5.30}$$

where the concentration of species A, for example, is denoted by $[A]$ and $k(T)$ is known as the reaction rate constant (which happens to be a strong function of temperature):

$$k(T) = A\sqrt{T} \exp -\frac{\hat{E}_a}{RT} \tag{5.31}$$

where A in this expression is a pre-exponential constant or frequency factor. For a slightly more complicated irreversible reaction with stoichiometric coefficients ν_i,

$$\nu_A A + \nu_B B \rightarrow \nu_C C + \nu_D D, \tag{5.32}$$

the reaction rate is given by

$$R_r = k(T)[A]^{\nu_A}[B]^{\nu_B}. \tag{5.33}$$

For this more complex reaction, the reaction rate constant is given by

$$k(T) = AT^{\beta} \exp -\frac{\hat{E}_a}{RT} \tag{5.34}$$

where β is a generalized temperature exponent that is usually small.

Now supposing the above reaction were reversible, as is most frequently the case,

$$\nu_A A + \nu_B B \longleftrightarrow \nu_C C + \nu_D D, \tag{5.35}$$

we write the rate of reaction as

$$R_r = R_{rf} - R_{rb} \tag{5.36}$$

to account for the individual rates of the forward and backward reactions:

$$R_{rf} = k_f(T)[A]^{\nu_A}[B]^{\nu_B} \qquad k_f(T) = A_f T^{\beta_f} \exp -\frac{\hat{E}_{af}}{RT}; \tag{5.37}$$

$$R_{rb} = k_b(T)[C]^{\nu_C}[D]^{\nu_D} \qquad k_b(T) = A_b T^{\beta_b} \exp -\frac{\hat{E}_{ab}}{RT}. \tag{5.38}$$

The rate of formation/consumption of a species, on a mole per unit volume basis, is given by

$$\frac{d\chi_i}{dt} = \pm \nu_i R_r. \tag{5.39}$$

The activation energies associated with the forward and backward reactions, $\hat{E}_{af}$ and $\hat{E}_{ab}$ are related via the enthalpy of reaction:

$$\hat{E}_{af} - \hat{E}_{ab} = \Delta H_r. \tag{5.40}$$

The activation energy represents a barrier; the higher the activation energy for a given direction, the higher the temperature must be before the reaction can proceed in that direction at any measurable rate.

An important relationship exists between the forward and backward reaction rate constants. At equilibrium,

$$\frac{d[\chi_i]}{dt} = 0 \tag{5.41}$$

Because the reaction rate is 0,

$$k_f \prod_{\text{react}} [\chi_i]^{\nu_i} - k_b \prod_{\text{prod}} [\chi_i]^{\nu_i} = 0. \tag{5.42}$$

This leaves us with the following expression linking kinetics to thermodynamics:

$$\frac{k_f(T)}{k_b(T)} = \frac{\prod_{\text{prod}}[\chi_i^*]^{\nu_i}}{\prod_{\text{react}}[\chi_i^*]^{\nu_i}} = K_C(T) \tag{5.43}$$

where the "*" signifies that the concentration is for the species in equilibrium. K_C is the equilibrium constant based on concentration and is related to K_p, the equilibrium constant based on partial pressures, as follows:

$$K_C(T) = \frac{\prod_{\text{prod}}[\chi_i^*]^{\nu_i}}{\prod_{\text{react}}[\chi_i^*]^{\nu_i}} = \frac{1}{(RT)^{\sum_\nu}} \frac{\prod_{\text{prod}}[p_i]^{\nu_i}}{\prod_{\text{react}}[p_i^*]^{\nu_i}} = \frac{1}{(RT)^{\sum_\nu}} K_p(T) \tag{5.44}$$

where $\sum_\nu$ is the "sum" over the stoichiometric coefficients with the stoichiometric coefficients of reactant species counted negatively. When the number of moles of product species is the same as the number of moles of reactant species, as is the case in the water-gas shift, $K_C(T) = K_p(T)$.

5.2.2 Kinetics of the Homogeneous Water-Gas Shift

The kinetics of the gas-phase water-gas shift will now be treated. In order to describe the kinetics of the overall reaction, the reaction rates of the individual elementary reactions must be determined. A list of elementary reactions that comprise an overall reaction is called a reaction mechanism, and the following is the reaction mechanism for the water-gas shift. The corresponding forward rate constant accompanies each elementary reaction.

1	$CO + OH \longleftrightarrow CO_2 + H$	$k_f = 4.4T^{1.5}\exp(373/T)$
2	$CO + O_2 \longleftrightarrow CO_2 + O$	$k_f = 2.5 \times 10^6 \exp(-24060/T)$
3	$CO + O + M \longleftrightarrow CO_2 + M$	$k_f = 53\exp(2285/T)$
4	$CO + HO_2 \longleftrightarrow CO_2 + OH$	$k_f = 1.5 \times 10^8 \exp(-11900/T)$
5	$H + O_2 \longleftrightarrow O + OH$	$k_f = 1.2 \times 10^{11}T^{-0.91}\exp(-8310/T)$
6	$H_2 + O \longleftrightarrow H + OH$	$k_f = 15T^2\exp(-3800/T)$
7	$O + H_2O \longleftrightarrow OH + OH$	$k_f = 1.5 \times 10^4 T^{1.14}\exp(-8680/T)$
8	$OH + H_2 \longleftrightarrow H + H_2O$	$k_f = 100T^{1.6}\exp(-1660/T)$
9	$O + HO_2 \longleftrightarrow O_2 + OH$	$k_f = 2.0 \times 10^7$
10	$H + HO_2 \longleftrightarrow OH + OH$	$k_f = 1.5 \times 10^8 \exp(-500/T)$
11	$H + HO_2 \longleftrightarrow H_2 + O_2$	$k_f = 2.5 \times 10^7 \exp(-350/T)$
12	$OH + HO_2 \longleftrightarrow H_2O + O_2$	$k_f = 2.0 \times 10^7$
13	$HO_2 + HO_2 \longleftrightarrow H_2O_2 + O_2$	$k_f = 2.0 \times 10^7$
14	$H + O_2 + M \longleftrightarrow HO_2 + M$	$k_f = 1.5 \times 10^3 \exp(-500/T)$
15	$OH + OH + M \longleftrightarrow H_2O_2 + M$	$k_f = 9100\exp(2550/T)$
16	$O + H + M \longleftrightarrow OH + M$	$k_f = 1.0 \times 10^4$
17	$O + O + M \longleftrightarrow O_2 + M$	$k_f = 1.0 \times 10^5/T$
18	$H + H + M \longleftrightarrow H_2 + M$	$k_f = 6.4 \times 10^5/T$
19	$H + OH + M \longleftrightarrow H_2O + M$	$k_f = 1.41 \times 10^{11}/T^2$

Determining the backward rate constants requires that the equilibrium constants of these 19 elementary reactions be known. The equilibrium constant of a given reaction is found by multiplying the equilibrium constants of formation of the product species and then dividing by the equilibrium constants of formation of the reactant species. These equilibrium constants are highly temperature dependent; a temperature at which to analyze the kinetics of the water-gas shift would have to be chosen in order to determine these constants. The forward activation energy of carbon-containing reactants tends to be relatively high, and so 1100K was chosen in order to observe measurable reaction rates. The 19 elementary reactions above contain 10 species in total; their equilibrium constants of formation at 1100K, obtained from the JANAF Thermochemistry Tables, are tabulated below.

CO	2.0496×10^{4}
CO_2	1.469×10^{8}
H	5.07×10^{-4}
H_2	1
H_2O	7.194×10^{3}
HO_2	8.62×10^{-2}
H_2O_2	2.281
O	1.84×10^{-4}
O_2	1
OH	3.531×10^{-1}

The equilibrium constants of the elementary reactions are then calculated as

$$K_C = \frac{\prod_{\text{prod}} K_{f,\chi_i}}{\prod_{\text{reac}} K_{f,\chi_i}} \frac{1}{(RT)^{\sum_\nu}} \tag{5.45}$$

where $\sum_\nu$ is sum of the stoichiometric coefficients of the product species minus the sum of the stoichiometric coefficients of the reactant species. The backward rate constant is then calculated as $k_b = k_f/K_C$. The equilibrium constants and corresponding rate constants for the 19 elementary reactions are tabulated below.

	Reaction	K_C	k_f	k_b
1	$CO + OH \longleftrightarrow CO_2 + H$	10.2911	2.2532×10^{5}	2.1895×10^{4}
2	$CO + O_2 \longleftrightarrow CO_2 + O$	1.3188	7.92×10^{-4}	6.0057×10^{-4}
3	$CO + O + M \longleftrightarrow CO_2 + M$	3.5623×10^{11}	423.08	1.1877×10^{-9}
4	$CO + HO_2 \longleftrightarrow CO_2 + OH$	2.9359×10^{4}	3004.8	0.1023
5	$H + O_2 \longleftrightarrow O + OH$	0.1281	1.073×10^{5}	8.3735×10^{5}
6	$H_2 + O \longleftrightarrow H + OH$	0.9729	$5.5.7357\times10^{5}$	5.8952×10^{5}
7	$O + H_2O \longleftrightarrow OH + OH$	0.0942	1.6455×10^{4}	1.747×10^{5}
8	$OH + H_2 \longleftrightarrow H + H_2O$	10.3295	1.6248×10^{6}	1.5731×10^{5}
9	$O + HO_2 \longleftrightarrow O_2 + OH$	2.2262×10^{4}	2×10^{7}	898.4
10	$H + HO_2 \longleftrightarrow OH + OH$	2852.9	9.521×10^{7}	33374
11	$H + HO_2 \longleftrightarrow H_2 + O_2$	22882	1.8187×10^{7}	794.8
12	$OH + HO_2 \longleftrightarrow H_2O + O_2$	2.3636×10^{5}	2×10^{7}	84.62
13	$HO_2 + HO_2 \longleftrightarrow H_2O_2 + O_2$	306.9805	2×10^{7}	65151
14	$H + O_2 + M \longleftrightarrow HO_2 + M$	1.5549×10^{6}	952.1	6.1232×10^{-4}
15	$OH + OH + M \longleftrightarrow H_2O_2 + M$	1.6731×10^{5}	9243	0.0552
16	$O + H + M \longleftrightarrow OH + M$	3.4616×10^{10}	1×10^{4}	2.8888×10^{-7}
17	$O + O + M \longleftrightarrow O_2 + M$	2.7013×10^{11}	90.9091	3.3654×10^{-10}
18	$H + H + M \longleftrightarrow H_2 + M$	3.5578×10^{10}	581.8182	1.6353×10^{-8}
19	$H + OH + M \longleftrightarrow H_2O + M$	3.6751×10^{11}	1.1653×10^{5}	3.1708×10^{-12}

The 19 reaction rate equations are as follows:

$$R_1 = k_{f1}[CO][OH] - k_{b1}[CO_2][H] \tag{5.46}$$

$$R_2 = k_{f2}[CO][O_2] - k_{b2}[CO_2][O] \tag{5.47}$$

$$R_3 = k_{f3}[CO][O] - k_{b3}[CO_2] \tag{5.48}$$

$$R_4 = k_{f4}[CO][HO_2] - k_{b4}[CO_2][OH] \tag{5.49}$$

$$R_5 = k_{f5}[H][O_2] - k_{b5}[O][OH] \tag{5.50}$$

$$R_6 = k_{f6}[H_2][O] - k_{b6}[H][OH] \tag{5.51}$$

$$R_7 = k_{f7}[O][H_2O] - k_{b7}[OH]^2 \tag{5.52}$$

$$R_8 = k_{f8}[OH][H_2] - k_{b8}[H][H_2O] \quad (5.53)$$

$$R_9 = k_{f9}[O][HO_2] - k_{b9}[O_2][OH] \quad (5.54)$$

$$R_{10} = k_{f10}[H][HO_2] - k_{b10}[OH]^2 \quad (5.55)$$

$$R_{11} = k_{f11}[H][HO_2] - k_{b11}[H_2][O_2] \quad (5.56)$$

$$R_{12} = k_{f12}[OH][HO_2] - k_{b12}[H_2O][O_2] \quad (5.57)$$

$$R_{13} = k_{f13}[HO_2]^2 - k_{b13}[H_2O_2][O_2] \quad (5.58)$$

$$R_{14} = k_{f14}[H][O_2] - k_{b14}[HO_2] \quad (5.59)$$

$$R_{15} = k_{f15}[OH]^2 - k_{b15}[H_2O_2] \quad (5.60)$$

$$R_{16} = k_{f16}[O][H] - k_{b16}[OH] \quad (5.61)$$

$$R_{17} = k_{f17}[O]^2 - k_{b17}[O_2] \quad (5.62)$$

$$R_{18} = k_{f18}[H]^2 - k_{b18}[H_2] \quad (5.63)$$

$$R_{19} = k_{f19}[H][OH] - k_{b19}[H_2O] \quad (5.64)$$

In the mechanism of 19 elementary reactions, there are 10 species: CO, OH, CO_2, O_2, O, HO_2, H, H_2O, and H_2O_2. The rates of production of these species are as follows:

$$\frac{d[CO]}{dt} = -R1 - R2 - R3 - R4 \quad (5.65)$$

$$\frac{d[OH]}{dt} = -R1 + R4 + R5 + R6 + 2R7 - R8 + R9 + 2R10 - R12 - 2R15 \quad (5.66)$$

$$+R16 - R19 \quad (5.67)$$

$$\frac{d[CO_2]}{dt} = R1 + R2 + R3 + R4 \quad (5.68)$$

$$\frac{d[O_2]}{dt} = -R2 - R5 + R9 + R11 + R12 + R13 - R14 + R17 \quad (5.69)$$

$$\frac{d[O]}{dt} = R2 - R3 + R5 - R6 - R7 - R9 - R16 - 2R17 \quad (5.70)$$

$$\frac{d[HO_2]}{dt} = -R4 - R9 - R10 - R11 - R12 - 2R13 + R14 \quad (5.71)$$

$$\frac{d[H]}{dt} = R1 - R5 + R6 + R8 - R10 - R11 - R14 - R16 - 2R18 - R19 \quad (5.72)$$

$$\frac{d[H2O]}{dt} = -R7 + R8 + R12 + R19 \quad (5.73)$$

$$\frac{d[H2O2]}{dt} = R13 + R15 \quad (5.74)$$

$$\frac{d[H2]}{dt} = -R6 - R8 + R11 + R18 \tag{5.75}$$

$$\tag{5.76}$$

A Matlab script was written to solve this set of ordinary differential equations for variable η (steam to gas ratio of the inlet stream). The script and associated files are included in the appendix; the plots generated by this script are shown in Figure 5.2. The figure shows that, at 1100 K in the gas-phase, the water-gas shift proceeds very slowly. The required residence time decreases with increasing η, but even at $\eta = 50$, over two minutes are required to reach a conversion of 98%. Over 113 moles of steam per mole of CO would be required to convert 99.5% of the CO.

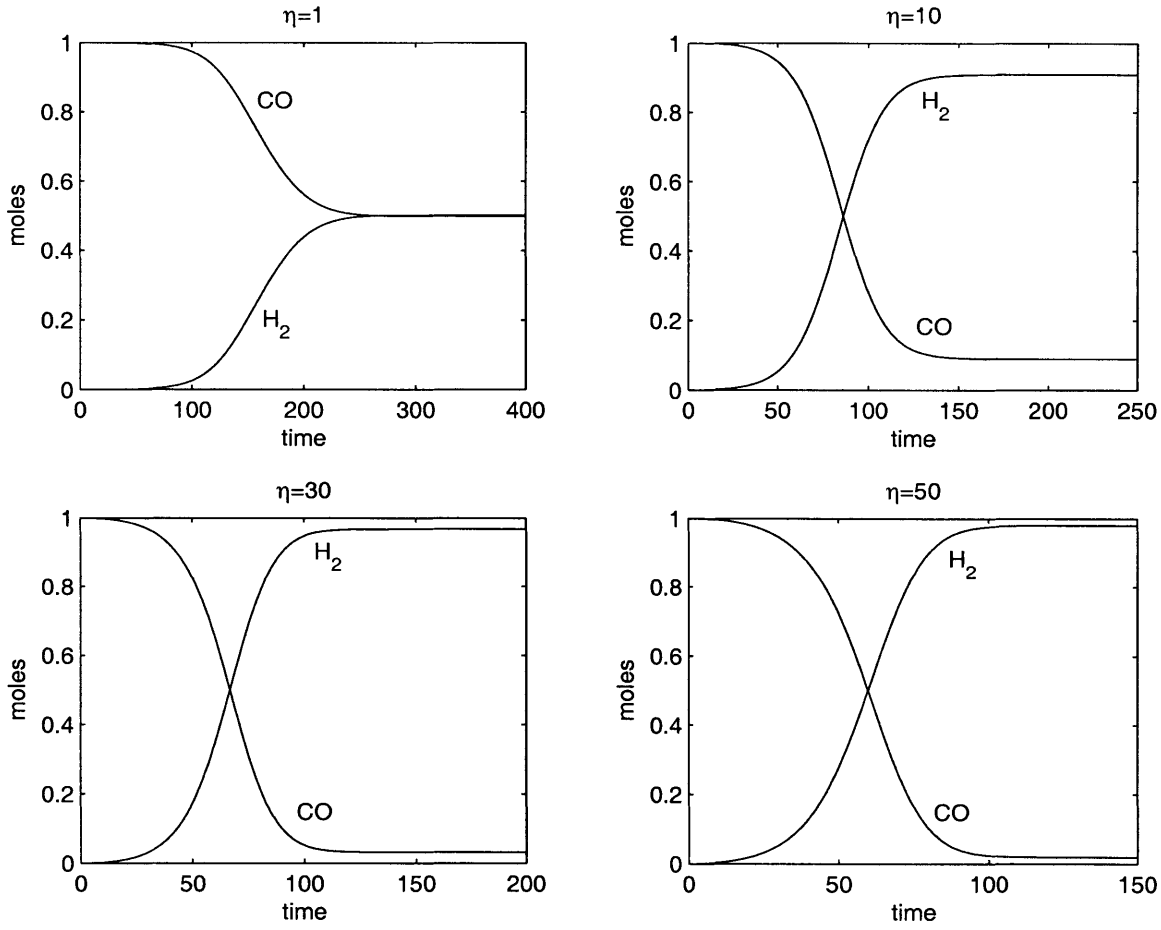

Figure 5.2: Illustration of how the moles of CO and H_2 vary with time as the water gas shift proceeds in the gas phase. At 1100 K, over 113 moles of steam would be required to convert 99.5% of the CO.

Figure 5.2 emphasizes the importance of catalysis for this reaction. Catalyzing the reaction would 1) lower the net activation energy of the reaction, lowering the temperature required to make reaction rates measurable, and 2) speed the reaction in the forward direction. A catalytic reaction involves species in the gas phase and also on the surface of the catalyst. A very different reaction mechanism would have to be written for the multiple-phase reaction, and the rate equation of each step in the mechanism would have to be confirmed using empirical data. Understanding the kinetics of a heterogeneous reaction relies heavily on experimentation, which will be the thrust of the future work. The following discussion of heterogeneous and catalytic kinetics creates a framework for this future work.

5.3 Heterogeneous and Catalytic Kinetics

The heterogeneous catalytic reaction of interest here is the sort that takes place at the interface between a solid surface and a gas, but it is also possible for catalytic reactions to take place at the interface between a solid and a liquid. The first step in a catalytic chain reaction is the adsorption of the gaseous molecules into the surface sites available for this purpose. The number of sites per unit area is a property of the catalyst surface. Adsorption processes can be physical (physisorption) or chemical (chemisorption), depending on the type of bond forming between the adsorbed gas molecule and the solid surface. Chemisorption requires more energy because it involves chemical bond formation. It is possible for a process to change the number of sites available for adsorption; a poison is a species that decreases the number of sites available, and a promoter is a species that increases the number of sites per unit area. Sulfur is a common poison for most catalysts, for example, and ceria is often used to promote ferro-chrome.

The following is the nomenclature to be used to describe a reaction in which a gaseous molecule $A_{(g)}$ is adsorbed into an open site to form an adsorbed molecule $A_{(s)}$:

$$A_{(g)} + * \longrightarrow A_{(S)}. \tag{5.77}$$

The energy balance for this reaction is expressed as an enthalpy of adsorption:

$$\Delta H_{ads} = h_{A_{(s)}} - h_{A_{(g)}}. \tag{5.78}$$

In order to conserve energy, this enthalpy is often assigned to the site: $h_* = \Delta H_{ads}$.

The free energy of adsorption, defined in much the same way as the enthalpy of adsorption, determines the equilibrium constant for the adsorption/desorption process. At equilibrium,

$$A_{(g)} + * \longleftrightarrow A_{(S)} \tag{5.79}$$

and

$$k_f[A_{(g)}][*] = k_b[A_{(s)}]. \tag{5.80}$$

The concentration-based equilibrium constant is

$$K_C = \frac{k_f}{k_b} = \frac{[A_{(s)}]}{[A_{(g)}][*]} \tag{5.81}$$

and the partial pressure based equilibrium constant is

$$K_p = \exp\left(\frac{-\Delta G_{ads}}{RT}\right) \tag{5.82}$$

where $\Delta G_{ads} = \Delta H_{ads} - T\Delta S_{ads}$. K_C is then expressed in terms of the free energy as

$$K_C = RT \exp\left(\frac{-\Delta G_{ads}}{RT}\right) \tag{5.83}$$

Adsorption and desorption processes are often faster than surface reactions and can be considered to be at partial equilibrium so that the equilibrium constant can be used to express the concentration of adsorbed species as a function of temperature and pressure. If Γ denotes the total number of sites per unit area of surface that can participate in reaction, then the $\Gamma = [A_{(s)}] + [*]$. The fraction of occupied sites at equilibrium is then

$$\theta_A = \frac{[A_{(s)}]}{\Gamma} = \frac{k_f[A_{(g)}]}{k_b + k_f[A_{(g)}]} = \frac{K_C[A_{(g)}]}{1 + K_C[A_{(g)}]}. \tag{5.84}$$

This last statement can be re-expressed in terms of the partial pressure of $A_{(g)}$ using the ideal gas

law to obtain what is known as the Langmuir adsorption isotherm:

$$\theta_A = \frac{\kappa P_A}{1 + \kappa P_A} \tag{5.85}$$

where $\kappa = K_C/RT$. The adsorption isotherm, along with the assumption that adsorption/desorption processes are at equilibrium, can be used to construct complex kinetic rate equations. For instance, if two species A and B adsorb onto a single surface according to Equation 5.79, $\Gamma = [A_{(s)}] + [B_{(s)}]$ and the fraction of sites occupied by each species is

$$\theta_A = \frac{K_{C,A}[A_{(g)}]}{1 + K_{C,A}[A_{(g)}] + K_{C,B}[B_{(g)}]}, \tag{5.86}$$

and

$$\theta_B = \frac{K_{C,B}[B_{(g)}]}{1 + K_{C,A}[A_{(g)}] + K_{C,B}[B_{(g)}]}. \tag{5.87}$$

These occupied site fractions can now be used to write down the Langmuir-Hinshelwood equation for the reaction rate of a surface reaction followed by desorption; that is, the products form and then leave the surface:

$$A_{(s)} + B_{(s)} \longrightarrow C_{(g)} + 2* \tag{5.88}$$

The rate of production is given by

$$\frac{[C_{(g)}]}{dt} = k_f[A_{(s)}][B_{(s)}] = \frac{k_f K_{C,A} K_{C,B} \Gamma^2 [A_{(g)}][B_{(g)}]}{1 + K_{C,A}[A_{(g)}] + K_{C,B}[B_{(g)}]}. \tag{5.89}$$

Chapter 6

Future Work

6.1 Kinetics

The kinetics of heterogeneous reactions are significantly more complex than the kinetics of homogeneous reactions. The relationships of the previous chapter will be used with empirical data to determine the rate of each step of an appropriate reaction mechanism for the water-gas shift reaction. The following mechanism is commonly accepted in literature:

$$CO + 2O* \longleftrightarrow CO_3 *_2 \tag{6.1}$$

$$CO_3*_2 \longleftrightarrow CO_3 * + * \tag{6.2}$$

$$CO_3* \longleftrightarrow CO_2 + O * \tag{6.3}$$

$$H_2O + * \longleftrightarrow H_2O * \tag{6.4}$$

$$H_2O * + O* \longleftrightarrow 2 * OH \tag{6.5}$$

$$2OH* \longleftrightarrow 2O * + H_2 \tag{6.6}$$

$$H_2O * + * \longleftrightarrow *OH + H * \tag{6.7}$$

$$2H* \longleftrightarrow H_2 + 2 * \tag{6.8}$$

$$\tag{6.9}$$

The bond strengths (activation energies) of each of these steps will have to be determined

experimentally in order to quantify the rate of production of each species in the mechanism. The rate model to be used will be specific to the environment in which the catalyst operates. The results of kinetic modeling by Ma and Lund, which assumed negligible effects of the partial pressure of hydrogen, yielded the following activation energies:

Species or Reaction	**Bond Strength or Activation Energy (kJ/mol)**
$O*$	578.0
CO_3*_2	724.5
CO_3*	642.7
H_2O*	59.1
$HO*$	353.0
$H*$	55.1
$CO + 2O* \longleftrightarrow CO_3*_2$	85.5
$CO_3*_2 \longleftrightarrow CO_3 + *$	12.3
$CO_3* \longleftrightarrow CO_2 + O*$	34.6
$H_2O + * \longleftrightarrow H_2O*$	0.0
$H_2O * + O* \longleftrightarrow 2 * OH$	47.5
$2OH* \longleftrightarrow 2O * + H_2$	3.4
$H_2O * + * \longleftrightarrow *OH + H*$	90.2
$2H* \longleftrightarrow H_2 + 2*$	35.5

In his presentation of experimental work, Lund noted that 99% of the surface was $O*$, which is consistent with this species having one of the largest bond energies. It is because the bond strengths of CO_3*_2, CO_3*, and $O*$ are the greatest of all species in this system that the carbon dioxide is known to so greatly inhibit the reaction. One of the goals of the kinetic modeling in this work is to determine how much catalyst could be saved if the $O*$ bond were weakened (with a ceria promoter which would lower the peak reduction temperature) in addition to removing both the hydrogen and carbon dioxide.

Once the kinetics of the heterogeneous reaction over ferro-chrome are better understood in an environment in which the partial pressures of hydrogen and carbon dioxide both play an important role, the reactor can be sized based on desired residence time and mass flow rate of reacting gases.

6.2 Mass Flow Through Membranes

The future work will also include a description of the mass transport of hydrogen and carbon dioxide across their respective permselective membranes. The following is a treatment for hydrogen; the treatment for the carbon dioxide would be congruous.

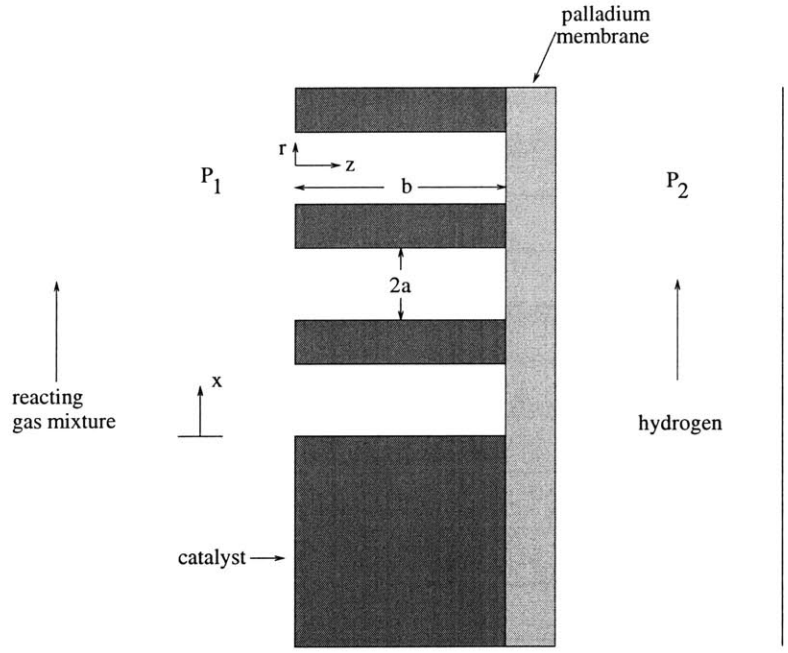

Figure 6.1: Sketch of catalyst pores with a palladium backing where P_1 and P_2 are H_2 partial pressures.

In the following analysis of the fluid flow, diffusional effects are ignored and the hydrogen is modeled as an ideal gas so that $P = \rho RT$, where $R = 4.157$ J/kg·K is the gas constant divided by the molecular weight. The flow of hydrogen through the palladium pore is expected to be low Reynold's number flow.

The velocity components are

$$\vec{v} =< v_z, v_r, v_\theta >$$

and the Navier-Stokes equation for the flow in the z direction is

$$\rho\left(\frac{\partial v_z}{\partial t} + v_z\frac{\partial v_z}{\partial z} + v_r\frac{\partial v_z}{\partial r} + \frac{v_\theta}{r}\frac{\partial v_z}{\partial \theta}\right) = -\frac{dp}{dz} + \mu\left(\frac{\partial^2 v_z}{\partial z^2} + \frac{1}{r}\frac{\partial}{\partial r}r\frac{\partial v_z}{\partial r} + \frac{1}{r^2}\frac{\partial v_z}{\partial \theta^2}\right). \tag{6.10}$$

The flow will be considered fully-developed and entrance effects will be neglected in this order-of-magnitude estimate. The flow rate is constant (in time) and is not a function of angular orientation. The Navier-Stokes equation thus reduces to

$$0 \approx -\frac{dp}{dz} + \frac{\mu}{r}\frac{\partial}{\partial r} r \frac{\partial v_z}{\partial r}. \tag{6.11}$$

The two boundary conditions for this second order differential equation are $v_z(r = a) = 0$ and $\partial v_z/\partial r = 0$ at $r = 0$. The solution is

$$v_z = -\frac{a^2}{4\mu}\frac{dp}{dz}\left(1 - \frac{r^2}{a^2}\right). \tag{6.12}$$

The volume flow rate is then

$$Q = \int_0^a -\frac{a^2}{4\mu}\frac{dp}{dz}\left(1 - \frac{r^2}{a^2}\right) 2\pi r dr = -\frac{\pi a^4}{8\mu}\frac{dp}{dz}. \tag{6.13}$$

Mass conservation gives

$$\rho Q = \dot{m} = \frac{P}{RT}\left(\frac{-\pi a^4}{8\mu}\frac{dp}{dz}\right) = \frac{-\pi a^4}{8\mu RT}\frac{d\left(p^2/2\right)}{dz} \tag{6.14}$$

or

$$\dot{m} = \frac{\pi a^4 \left(P_1^2 - P_2^2\right)}{16\mu RTb} = \frac{\pi a^4 P_2^2}{16\mu RTb}\left(\frac{P_1^2}{P_2^2} - 1\right) \tag{6.15}$$

where P_2 is small. It is interesting to note that $\dot{m} \propto 1/T$. This relationship points to a trade off between favorable kinetics, which occur at high temperatures, and high flow rates of hydrogen through the membrane, which occur at low temperatures. At the start of the reactor, near $x = 0$, $P_1 >> P_2$ and

$$\dot{m} \approx \frac{\pi a^4 P_1^2}{16\mu RTb}. \tag{6.16}$$

Similarly, at $x = L$ (see Figure 2.3), the pressure differential is expected to be minimal, $P_2 = P_1 - \Delta P$. $P_2^2 \approx P_1^2 - 2P_1\Delta P$ and at x near L,

$$\dot{m} \approx \frac{\pi a^4 P_1 \Delta P}{8\mu RTb}. \tag{6.17}$$

How $\dot{m}$ varies with x depends on how the partial pressure of hydrogen changes as the gas mixture travels from one end of the reactor to the other and will be determined once the kinetics of the heterogeneous reaction are better understood.

Chapter 7

Conclusions

This body of work suggests a unique design option for a compact and efficient catalytic reactor for the water-gas shift. Specifically, this work recommends that a ferro-chrome catalyst, an industry standard for the high temperature, non-membrane shift reactor, be employed in a duo-selecting membrane reactor in which both products of the water-gas shift reaction, hydrogen and carbon dioxide, are selectively removed. Ferro-chrome is known for its fast kinetics at high temperatures in an environment when the partial pressures of both hydrogen and carbon dioxide are high; ferro-chrome is also understood to be significantly less efficient in an environment when the partial pressure of either hydrogen or carbon dioxide is low. For this reason, ferro-chrome is not recommended for use in a traditional membrane reactor. The potential benefit of a duo-selecting membrane reactor is that the partial pressures of hydrogen and carbon dioxide are both low, and the ratio of the two is comparable to the ratio P_{H_2}/P_{CO_2} in a standard non-membrane shift reactor. The behavior of ferro-chrome in such an environment is not yet well-studied.

This work is an assembly of thermodynamic and kinetic models. The thermodynamic model compares the hydrogen yield of a reactor operating isothermally to that of a reactor operating adiabatically. The results of this modeling exercise show that 95% hydrogen yields are realized for steam to gas ratios as low as 2 in a reactor operating isothermally at 600K, which is the minimum operating temperature of the catalyst. At 750K, the maximum operating temperature of the catalyst, comparable hydrogen yields are realized for steam to gas ratios above 9. One disadvantage to running the reactor at the lower temperature is that significantly more entropy is

generated; at 600K with a steam to gas ratio of 2, approximately 20 J/K are generated per mole of converted CO, while at 750K with a steam to gas ratio of 9, the reactor generates less than 1 J/K per mole of converted CO. The generated entropy is responsible for lost work and could result in excessive power requirements. Another potential disadvantage to running the reactor isothermally at the lower temperature is that slightly more heat must be removed from the reactor, approximately 38 kJ/mole of CO at 600K versus 34 kJ/mole of CO at 750K. Because the aim is to minimize the size of the reactor, care must be taken in designing a reservoir to which this "waste heat" would be transferred. Flowing cooling water is recommended for this purpose, but the details of this heat transfer problem are not explored in this body of work. In the adiabatic mode of operation, at least 6 moles of steam are required per mole of CO in order to keep the flame temperature below 750K and the hydrogen yield in this case is typically at least 0.5% lower than in the isothermal case at 750K.

The kinetic modeling exercise explores the gas-phase kinetics of the water gas shift in detail and describes, in general, the kinetics of heterogeneous and catalytic reactions. This work suggests that ferro-chrome operate in an environment that has not previously been studied, and understanding the kinetics of the water-gas shift over ferro-chrome in this environment requires extensive experimentation. This issue is discussed in the chapter on Future Work.

Other elements of future work include: 1) analyzing the flow of gases through the membranes, 2) determining the mass flow rate of sweep gas on the permeate sides of the membrane, and 3) after sufficient experimental work that will lead to a quantitative description of catalyst behavior and surface kinetics, sizing the reactor.

Chapter 8

References

1. Spath, P.L., Mann, M.K., "Life Cycle Assessment of Hydrogen Production via Natural Gas Steam Reforming," National Renewable Engergy Laboratory, Golden, CO, NREL/TP-570-27637, 2001.

2. Houghton, J.T. Meira Filho, L.G., Callandeer, M.A., Harris, N., Kattenberg, A., Maskell, K., eds. (1996). *Climate Change 1995. The Science of Climate Change.* Published for the Intergovernmental Panel on Climate Change. New York: Cambridge University Press.

3. Heung, K., "Separation Membrane Development," in the *Hydrogen, Fuel Cells, and Infrastructure Technologies*, DOE Progress Report, FY 2002, II.C.9.

4. Nenoff, T., "Defect-Free Thin Film Membranes for H_2 Separation and Isolation," in the *Hydrogen, Fuel Cells, and Infrastructure Technologies*, DOE Progress Report, FY 2002, II.C.10.

5. Li, N.N., Drioli, E., Ho, W.S.W., Lipscomb, G.G., Advanced Membrane Technology, from the Annals of the New York Academy of Sciences, **984**, (2003).

6. Chen, C.M., Carolan, M.F., Rynders, S.W., "ITM Syngas and ITM H_2: Engineering of Ceramic Membrane Reactor Systems for Converting Natural Gas to Hydrogen and Synthesis Gas for Liquid Transportation Fuels" in the *Hydrogen, Fuel Cells, and Infrastructure Technologies*, DOE Progress Report, FY 2002, II.C.5.

7. Ma, D., Lund, C.R.F., "Assessing High-Temperature Water-Gas Shift Membrane Reactors," *Ind. Eng. Chem. Res.*, **42**, pp. 711-717, (2003).

8. Muradov, N., "Thermocatalytic CO_2-Free Production of Hydrogen from Hydrocarbon Fuels," in the *Hydrogen, Fuel Cells, and Infrastructure Technologies* DOE Progress Report, FY 2002, II.C.3.

9. James, B.D., Myers, D.B., Ariff, G.D., Lettow, J.S., Thomas, C.E., Kuhn, R.C., "Distibuted Hydrogen Fueling Systems Analysis: Cost and Performance Comparison of Stationary Hydrogen Fueling Systems," in the *Hydrogen, Fuel Cells, and Infrastructure Technologies* DOE Progress Report, FY 2002, II.E.4.

10. Armor, J.N., "Catalysis with Permselective Inorganic Membranes," *J. Appl. Catalysis*, **49**, pp. 1-25, (1989).

11. Buxbaum, R., "Membrane Reactors, Fundamental and Commercial Advantages, E.G. for Methanol Reforming," presented at the 15^{th} BCC Membrane Planning Conference, Newton, Massachusetts, October 27-29, 1997 and at the Canadian AICHE Membrane Separations Meeting, Calgary Alberta, August 1997.

12. Amphlett, J.C., Creber, K.A.M., Davis, J.M., Mann, R.F., Peppley, B.A., Stokes, D.M., "Hydrogen Production by Steam Reforming of Methanol for Polymer Electrolyte Fuel Cells." *Int. J. Hydrogen Energy*, **19**, pp. 131-137, (1994).

13. Bohlbro, H., "An Investigation of the Conversion of Carbon Monoxide with Water Vapour Over Iron Oxide Based Catalysts," Haldor-Topsoe, Gjellerup, Copenhagen, 1969.

14. Brooks, K.P., Davis, J.M., Fischer, C.M., Heintzelman, A.R., King, D.L., Stenkamp, V.S., TeGrotenhuis, W.E., Wegeng, R.S., Whyatt, G.A., Pederson, L.R., "Microchannel Fuel Processor Development," in the *Hydrogen, Fuel Cells, and Infrastructure Technologies* DOE Progress Report, FY 2002, IV.C.4.

15. Betta, R.D., "Plate-Based Fuel Processing System," in the *Hydrogen, Fuel Cells, and Infrastructure Technologies* DOE Progress Report, FY 2002, IV.C.5.

16. Thompson, L., "Fuel Processors for PEM Fuel Cells," in the *Hydrogen, Fuel Cells, and Infrastructure Technologies* DOE Progress Report, FY 2002, IV.C.6.

17. Karnik, S.V., Hatalis, M.K., Kothare, M.V., "Palladium based Micro-Membrane for Water Gas Shift Reaction and Hydrogen Gas Separation," in the proceedings of the 5^{th} International Conference on Microreaction Technology (IMRET 5), Strasbourg, France, May 27-30, 2001.

Appendix A

Codework

A.1 Thermodynamic Model

A.1.1 Isothermal Mode of Operation

```
% isotherm.m
% AliciA Jillian J Hardy
% 30 March 2004

% This script file plots the performance curve for the reactor
% operating isothermally. The equilibrium composition of the stream
% is determined by the equilibrium constant for the water-gas
% shift, and the entropy generated between the inlet and outlet of
% the reactor is calculated.

clear

T = 750; % K. This temperature can vary only between 600 and 750K.
eta = 1; % steam to gas ratio.

% Expression for the equilibrium constant was obtained from problem
```

```
% set 5 in Prof. Ghoniem's course on Energy conversion systems.

KC = 103943/(exp(-4949.17*(1/T-1/298)));

% The expression for beta is a quadratic. The quadratic will be
% solved for values of eta between 1 and 20.

eta = 1;
counter = 1;

while eta < 20.25,
  A = 1-KC;
  B = KC*(eta+1);
  C = -1*eta*KC;

  beta = (-1*B+sqrt(B^2-4*A*C))/2/A;

  coeffs % Obtains the coefficients of the reaction.
  deltaHcalc % Calculates the heat transfer out of the reactor.
  Sgencalc %Calculates the entropy generated

  while Sgen(counter) < 0,
    beta = beta - 0.001;
    coeffs
    deltaHcalc
    Sgencalc
  end

  conversion(counter) = beta;
  ratio(counter) = eta;
```

```
  eta = eta+1;
  counter = counter + 1;
end

%plot(ratio, conversion)
%plot(ratio, Sgen)
%plot(ratio, deltaH)
```

```
% Sgencalc.m
% AliciA Jillian J Hardy
% 30 March 2004

% This script file, to be used with isotherm.m, calculates the
% entropy generated in the reactor operating isothermally

% SHOMATE EQUATION COEFFICIENTS

A = [30.09200 25.56759 24.99735 33.066178];
B = [6.832514 6.096130 55.18696 -11.363417];
C = [6.793435 4.054656 -33.69137 11.432816];
D = [-2.534480 -2.671301 7.948387 -2.772874];
E = [0.082139 0.131021 -0.136638 -0.158558];
F = [-250.8810 -118.0089 -403.6075 -9.980797];
G = [223.3967 227.3665 228.2431 172.707974];
H = [-241.8264 -110.5271 -393.5224 0.0];

Ptot = 6; % atm. This number can change, it is assumed for now.
ntot = eta + 1;
R = 8.314; % J/mol K
t = T/1000;
soft = ...
    A.*log(t)+B.*t+C.*t.^2./2+D.*t.^3./3-E./2./t.^2+G;

% incoming entropy

sH2Oin = soft(1) + 188.835 - R*log(nH2Oin/ntot*Ptot);
sCOin = soft(2) + 197.66 - R*log(nCOin/ntot*Ptot);
```

```
Sin = nH2Oin*sH2Oin + nCOin*sCOin;

% outgoing entropy

sH2Oout = soft(1) + 188.835 - R*log(nH2Oout/ntot*Ptot);
sCOout = soft(2) + 197.66 - R*log(nCOout/ntot*Ptot);
sCO2out = soft(3) + 213.785 - R*log(nCO2out/ntot*Ptot);
sH2out = soft(4) + 130.68 - R*log(nH2out/ntot*Ptot);

Sout = nH2Oout*sH2Oout + nCOout*sCOout + nCO2out*sCO2out + ...
    nH2out*sH2out;


deltaS(counter) = Sout - Sin;

Sgen(counter) = deltaS(counter)-deltaH(counter)*1000/T;
```

```
% deltaHcalc.m
% AliciA Jillian J Hardy
% 30 March 2004

% This script file, to be used with isotherm.m, calculates the heat
% transfer out of the reactor operating isothermally.

% SHOMATE EQUATION COEFFICIENTS

A = [30.09200 25.56759 24.99735 33.066178];
B = [6.832514 6.096130 55.18696 -11.363417];
C = [6.793435 4.054656 -33.69137 11.432816];
D = [-2.534480 -2.671301 7.948387 -2.772874];
E = [0.082139 0.131021 -0.136638 -0.158558];
F = [-250.8810 -118.0089 -403.6075 -9.980797];
G = [223.3967 227.3665 228.2431 172.707974];
H = [-241.8264 -110.5271 -393.5224 0.0];



t = T/1000;
hoft = A.*t+B.*t.^2./2+C.*t.^3./3+D.*t.^4./4-E./t+F-H;

% incoming enthalpy

hH2Oin = hoft(1) -241.826;
hCOin = hoft(2) - 110.53;
Hin = nH2Oin*hH2Oin + nCOin*hCOin;

% outgoing enthalpy
```

```
hH2Oout = hoft(1) -241.826;
hCOout = hoft(2) - 110.53;
hCO2out = hoft(3) - 393.51;
hH2out = hoft(4); % no heat of formation for the elements
Hout = nH2Oout*hH2Oout + nCOout*hCOout + nCO2out*hCO2out + ...
    nH2out*hH2out;


deltaH(counter) = Hout-Hin;
```

```
% coeffs.m
% AliciA Jillian J Hardy
% 30 March 2004

% This script file, to be used with isotherm.m, obtains the
% coefficients of the reaction based on equilibrium conversion.

nH2out = beta;
nCOout = 1-beta;
nCO2out = beta;
nH2Oout = eta - beta;

nH2in = 0;
nCOin = 1;
nCO2in = 0;
nH2Oin = eta;
```

A.1.2 Adiabatic Mode of Operation

```
% calladiab.m
% AliciA Jillian J Hardy
% 31 March 2004

% This script simply calls the routine adiabatic.m for changing
% values of eta, the steam to gas ratio.

clear

Tin = 600; % K. This will always be the case.
Tout = 600; % K. This starts the iteration.
eta = 6; % steam to gas ratio.
tolerance = 0.001; % to be used in the iteration.
counter = 1;

while eta < 20.25,

  adiabatic
  counter
  Tad(counter) = Tout;
  ratio(counter) = eta;
  deltaHplot(counter) = deltaH;
  Sgenplot(counter) = Sgen;
  conversion(counter) = beta;

  eta = eta + .25;
  counter = counter + 1;
```

```
end

% Now compare the adiabatic conversions to the equilibrium
% conversions at the adiabatic temperature.

counter = 1

while counter < 58
  Tout = Tad(counter);
  eqbeta
  conversioneq(counter) = beta;
  counter = counter + 1;
end
```

```
% adiabatic.m
% AliciA Jillian J Hardy
% 30 March 2004

% This script file plots the performace curve for the reactor
% operating adiabatically. The extent of reaction and adiabatic flame
% temperatures are obtained iteratively using the first and second
% laws of thermodynamics.

% Get the reaction stoichiometry based on equilibrium conversion.

eqbeta
coeffs

% Apply the first and second laws of thermodynamics to the
% reaction.

deltaHcalc
deltaScalc

% Check that the heat of reaction is 0 and that the entropy
% generated is positive. First try all outlet temperatures in the
% range (600 to 750K) for the equilibrium stoichiometry. If no
% temperature satisfies the requirements, lower the extent of
% reaction and then search again for an adiabatic flame temperature
% in range.

while abs(deltaH) > tolerance,
  if Tout < 750
    Tout = Tout + 0.01;
```

```
  else
    break
  end
  eqbeta
  coeffs
  deltaHcalc
  deltaScalc
  if Sgen < 0
    deltaH = 5*tolerance;
  end
end

% at this point we have tried all temperatures at the equilibrium
% conversion. Now try less than equilibrium conversions.

while abs(deltaH) > tolerance,
  if beta > 0
    beta = beta - 0.001;
  else
    break
  end
  if beta < 0
    beta = 0;
    break
  end
  Tout = 600; % K. Restart the iteration

  coeffs
  deltaHcalc
  deltaScalc
```

```
  while abs(deltaH) > tolerance,
    if Tout < 750
      Tout = Tout + 0.01;
    else
      break
    end
    coeffs
    deltaHcalc
    deltaScalc
    if Sgen < 0
      deltaH = 5*tolerance;
    end
  end
end
```

```
% deltaScalc.m
% AliciA Jillian J Hardy
% 30 March 2004

% This script file, to be used with the newest version of adiabatic.m,
% calculates the entropy generated in the reactor operating
% adiabatically.

% SHOMATE EQUATION COEFFICIENTS

A = [30.09200 25.56759 24.99735 33.066178];
B = [6.832514 6.096130 55.18696 -11.363417];
C = [6.793435 4.054656 -33.69137 11.432816];
D = [-2.534480 -2.671301 7.948387 -2.772874];
E = [0.082139 0.131021 -0.136638 -0.158558];
F = [-250.8810 -118.0089 -403.6075 -9.980797];
G = [223.3967 227.3665 228.2431 172.707974];
H = [-241.8264 -110.5271 -393.5224 0.0];

Ptot = 6; % atm. This number can change, it is assumed for now.
ntot = eta + 1;
R = 8.314; % J/mol K

% incoming entropy

t = Tin/1000;
soft = ...
    A.*log(t)+B.*t+C.*t.^2./2+D.*t.^3./3-E./2./t.^2+G;

sH2Oin = soft(1) + 188.835 - R*log(nH2Oin/ntot*Ptot);
```

```
sCOin = soft(2) + 197.66 - R*log(nCOin/ntot*Ptot);

Sin = nH2Oin*sH2Oin + nCOin*sCOin;

% outgoing entropy

t = Tout/1000;
soft = ...
    A.*log(t)+B.*t+C.*t.^2./2+D.*t.^3./3-E./2./t.^2+G;

sH2Oout = soft(1) + 188.835 - R*log(nH2Oout/ntot*Ptot);
sCOout = soft(2) + 197.66 - R*log(nCOout/ntot*Ptot);
sCO2out = soft(3) + 213.785 - R*log(nCO2out/ntot*Ptot);
sH2out = soft(4) + 130.68 - R*log(nH2out/ntot*Ptot);

Sout = nH2Oout*sH2Oout + nCOout*sCOout + nCO2out*sCO2out + ...
    nH2out*sH2out;


deltaS = Sout - Sin;

Sgen = deltaS;
```

```
% deltaHcalc.m
% AliciA Jillian J Hardy
% 30 March 2004

% This script file, to be used with the newest version of adiabatic.m,
% calculates the heat of reaction, which should be 0 in the
% adiabatic case.

% SHOMATE EQUATION COEFFICIENTS

A = [30.09200 25.56759 24.99735 33.066178];
B = [6.832514 6.096130 55.18696 -11.363417];
C = [6.793435 4.054656 -33.69137 11.432816];
D = [-2.534480 -2.671301 7.948387 -2.772874];
E = [0.082139 0.131021 -0.136638 -0.158558];
F = [-250.8810 -118.0089 -403.6075 -9.980797];
G = [223.3967 227.3665 228.2431 172.707974];
H = [-241.8264 -110.5271 -393.5224 0.0];

% incoming enthalpy

t = Tin/1000;
hoft = A.*t+B.*t.^2./2+C.*t.^3./3+D.*t.^4./4-E./t+F-H;

hH2Oin = hoft(1) -241.826;
hCOin = hoft(2) - 110.53;
Hin = nH2Oin*hH2Oin + nCOin*hCOin;

% outgoing enthalpy
```

```
t = Tout/1000;
hoft = A.*t+B.*t.^2./2+C.*t.^3./3+D.*t.^4./4-E./t+F-H;

hH2Oout = hoft(1) -241.826;
hCOout = hoft(2) - 110.53;
hCO2out = hoft(3) - 393.51;
hH2out = hoft(4); % no heat of formation for the elements
Hout = nH2Oout*hH2Oout + nCOout*hCOout + nCO2out*hCO2out + ...
    nH2out*hH2out;


deltaH = Hout-Hin;
```

```
% eqbeta.m
% AliciA Jillian J Hardy
% 30 March 2004

% This script, to be used with the newest version of adiabatic.m,
% finds the equilibrium extent of reaction based on outlet temperature.

% Expression for the equilibrium constant was obtained from problem
% set 5 in Prof. Ghoniem's course on Energy conversion systems.

KC = 103943/(exp(-4949.17*(1/Tout-1/298)));

% The expression for beta is a quadratic. The quadratic will be
% solved for values of eta between 1 and 20.

A = 1-KC;
B = KC*(eta+1);
C = -1*eta*KC;

beta = (-1*B+sqrt(B^2-4*A*C))/2/A;
\newpage
% coeffs.m
% AliciA Jillian J Hardy
% 30 March 2004

% This file, to be used with the newest version of adiabatic.m,
% provides the relavant stoichiometry of the reaction.

nH2in = 0;
nCO2in = 0;
```

```
nH2Oin = eta;
nCOin = 1;

nH2out = beta;
nCO2out = beta;
nCOout = 1-beta;
nH2Oout = eta - beta;
```

A.2 Kinetic Model

```
% reaction.m
% AliciA Jillian J Hardy
% 24 March 2004

% This script file ultimately plots the nonlinear differential
% equations for problem 1 in pset 5.

clear

eta = 50; % steam to gas ratio. 113.5 required to produce 0.995
            % mol H2
P = 10; % atm. This value is varied by hand
R = 8.314; % J/mol K
T = 1100; % K. This number does not change
to = 0; % start time
tf = 150; % end time, seconds
step = 1; % time step

% The initial conditions are provided as follows

ntot = eta + 1;
rho = P/R/T*10^5;
concCO = rho/ntot; % concentration is mole fraction x density in mol/Vol.
concH2O = eta*rho/ntot;

% xo = [concCO 0 0 0 0 0 0 concH2O 0 0];
xo = [1 0 0 0 0 0 0 eta 0 0];
```

```
% Now solve the ODEs using the calculated values of kf and kb for
% the 19 rate equations

[t,x] = ode23tb('rate1100',[to:step:tf],xo);
plot(t,x)
xlabel('time')
ylabel('moles')
% ylabel('concentration fraction')
% legend('CO', 'OH', 'CO2', 'O2', 'O', 'HO2', 'H', 'H2O', 'H2O2', 'H2')
```

```
% rate1100.m
% AliciA Jillian J Hardy
% 1 April 2004

% This script file represents the function to be run in order to
% determine the mole fractions of the various species in the gas
% phase

% R1 = kf1*[CO]*[OH]-kb1*[CO2]*[H]
% R2 = kf2*[CO]*[O2]-kb2*[CO2]*[O]
% R3 = kf3*[CO]*[O]-kb3*[CO2]
% R4 = kf4*[CO]*[HO2]-kb4*[CO2]*[OH]
% R5 = kf5*[H]*[O2]-kb5*[O]*[OH]
% R6 = kf6*[H2]*[O]-kb6*[H]*[OH]
% R7 = kf7*[O]*[H2O]-kb7*[OH]*[OH]
% R8 = kf8*[OH]*[H2]-kb8*[H]*[H2O]
% R9 = kf9*[O]*[HO2]-kb9*[O2]*[OH]
% R10 = kf10*[H]*[HO2]-kb10*[OH]*[OH]
% R11 = kf11*[H]*[HO2]-kb11*[H2]*[O2]
% R12 = kf12*[OH]*[HO2]-kb12*[H2O]*[O2]
% R13 = kf13*[HO2]*[HO2]-kb13*[H2O2]*[O2]
% R14 = kf14*[H]*[O2]-kb14*[HO2]
% R15 = kf15*[OH]*[OH]-kb15*[H2O2]
% R16 = kf16*[H]*[O]-kb16*[OH]
% R17 = kf17*[O]*[O]-kb17*[O2]
% R18 = kf18*[H]*[H]-kb18*[H2]
% R19 = kf19*[H]*[OH]-kb19*[H2O]

% x(1) is CO
% x(2) is OH
```

```
% x(3) is CO2
% x(4) is O2
% x(5) is O
% x(6) is HO2
% x(7) is H
% x(8) is H2O
% x(9) is H2O2
% x(10) is H2

function xdot = rate1100(t,x)
  xdot(1,1) = -1*(2.25e5*x(1)*x(2)-21895*x(3)*x(7)) - ...
      (7.92e4*x(1)*x(4)-6e4*x(3)*x(5)) - ...
      (423*x(1)*x(5)-1.2e-9*x(3)) - ...
      (3005*x(1)*x(6)-.1023*x(3)*x(2));

  xdot(2,1) = -1*(2.25e5*x(1)*x(2)-21895*x(3)*x(7)) + ...
      (3005*x(1)*x(6)-.1023*x(3)*x(2)) + ...
      (1.07e5*x(7)*x(4)-8.3735e5*x(5)*x(2)) + ...
      (5.74e5*x(10)*x(5)-5.9e5*x(7)*x(2)) + ...
      2*(16455*x(5)*x(8)-1.75e5*x(2)*x(2)) - ...
      (1.625e6*x(2)*x(10)-1.6e5*x(7)*x(8)) + ...
      (2e7*x(5)*x(6)-898.4*x(4)*x(2)) + ...
      2*(9.5e7*x(7)*x(6)-33374*x(2)*x(2)) - ...
      (2e7*x(2)*x(6)-84.62*x(8)*x(4)) - ...
      2*(9243*x(2)*x(2)-.0552*x(9)) + ...
      (1e4*x(7)*x(5)-2.9e-7*x(2)) - ...
      (1.1653e5*x(7)*x(2)-3.171e-12*x(8));

  xdot(3,1) = (2.25e5*x(1)*x(2)-21895*x(3)*x(7)) + ...
      (7.92e4*x(1)*x(4)-6e4*x(3)*x(5)) + ...
```

```
    (423*x(1)*x(5)-1.2e-9*x(3)) + ...
    (3005*x(1)*x(6)-.1023*x(3)*x(2));

xdot(4,1) = -1*(7.92e4*x(1)*x(4)-6e4*x(3)*x(5)) - ...
    (1.07e5*x(7)*x(4)-8.3735e5*x(5)*x(2)) + ...
    (2e7*x(5)*x(6)-898.4*x(4)*x(2)) ...
    + (1.82e7*x(7)*x(6)-794.8*x(10)*x(4)) + ...
    (2e7*x(2)*x(6)-84.62*x(8)*x(4)) + ...
    (2e7*x(6)*x(6)-65151*x(9)*x(4)) - ...
    (952*x(7)*x(4)-6.1232e-4*x(6)) + (90.91*x(5)*x(5)-3.4e-10*x(4));

xdot(5,1) = (7.92e4*x(1)*x(4)-6e4*x(3)*x(5)) - ...
    (423*x(1)*x(5)-1.2e-9*x(3)) + ...
    (1.07e5*x(7)*x(4)-8.3735e5*x(5)*x(2)) - ...
    (5.74e5*x(10)*x(5)-5.9e5*x(7)*x(2)) - ...
    (16455*x(5)*x(8)-1.75e5*x(2)*x(2)) ...
    - (2e7*x(5)*x(6)-898.4*x(4)*x(2)) - ...
    (1e4*x(7)*x(5)-2.9e-7*x(2)) - ...
    2*(90.91*x(5)*x(5)-3.4e-10*x(4));

xdot(6,1) = -1*(3005*x(1)*x(6)-.1023*x(3)*x(2)) - ...
    (2e7*x(5)*x(6)-898.4*x(4)*x(2)) - ...
    (9.5e7*x(7)*x(6)-33374*x(2)*x(2)) - ...
    (1.82e7*x(7)*x(6)-794.8*x(10)*x(4)) - ...
    (2e7*x(2)*x(6)-84.62*x(8)*x(4)) - ...
    2*(2e7*x(6)*x(6)-65151*x(9)*x(4)) + ...
    (952*x(7)*x(4)-6.1232e-4*x(6));

xdot(7,1) = (2.25e5*x(1)*x(2)-21895*x(3)*x(7)) - ...
    (1.07e5*x(7)*x(4)-8.3735e5*x(5)*x(2)) + ...
```

```
    (5.74e5*x(10)*x(5)-5.9e5*x(7)*x(2)) + ...
    (1.625e6*x(2)*x(10)-1.6e5*x(7)*x(8)) - ...
    (9.5e7*x(7)*x(6)-33374*x(2)*x(2)) - ...
    (1.82e7*x(7)*x(6)-794.8*x(10)*x(4)) - ...
    (952*x(7)*x(4)-6.1232e-4*x(6)) ...
    - (1e4*x(7)*x(5)-2.9e-7*x(2)) - ...
    2*(582*x(7)*x(7)-1.64e-8*x(10)) - ...
    (1.1653e5*x(7)*x(2)-3.171e-12*x(8));

xdot(8,1) = -1*(16455*x(5)*x(8)-1.75e5*x(2)*x(2)) + ...
    (1.625e6*x(2)*x(10)-1.6e5*x(7)*x(8)) + ...
    (2e7*x(2)*x(6)-84.62*x(8)*x(4)) + ...
    (1.1653e5*x(7)*x(2)-3.171e-12*x(8));

xdot(9,1) = (2e7*x(6)*x(6)-65151*x(9)*x(4)) + ...
    (9243*x(2)*x(2)-.0552*x(9));

xdot(10,1) = -1*(5.74e5*x(10)*x(5)-5.9e5*x(7)*x(2)) - ...
    (1.625e6*x(2)*x(10)-1.6e5*x(7)*x(8)) + ...
    (1.82e7*x(7)*x(6)-794.8*x(10)*x(4)) + ...
    (582*x(7)*x(7)-1.64e-8*x(10));
```